Electronic Supplementary Information (ESI)

1. General

All reactions were carried out under an inert atmosphere by applying a positive pressure of argon using oven-dried glassware. Dichloromethane (DCM) was distilled from calcium hydride. 1,2-Dichlorobenzene (1,2-DCB) was distilled from phosphorus pentoxide (P_2O_5). Flash chromatography (FC) and plug filtrations were carried out with silica gel 60N (particle size 0.040–0.050 mm; Kanto Chemical). Thin-layer chromatography (TLC) was conducted on aluminum sheets coated with silica gel 60 F254 obtained from Merck; visualization was achieved with a UV lamp (254 or 365 nm). Analytical high-performance column chromatography (HPLC) was run on a JASCO chromNAVI system equipped with a JASCO LC-Net II interface, a JASCO PU-2080 pump, a JASCO UV-2075plus UV-detector (330 nm) and a Buckyprep column (Nacalai Tesque; 40ºC in a column oven JASCO CO-2060plus) at flow rate of 1.0 mL min^{-1} with eluent of toluene/*n*-hexane 1:2 or 1:1 (v/v). Preparative HPLC was performed using a chromatograph (LC-918; Japan Analytical Industry Co.) that was monitored using UV absorption at 330 nm. 1D and 2D NMR spectra were measured on a JEOL JNM-ECX400P spectrometer (400 MHz) at room temperature unless otherwise stated. Chemical shifts δ are given in ppm relative to tetramethylsilane (TMS) and were referenced to internal TMS or residual non-deuterated solvent for ^{1}H and ^{13}C NMR spectra. Infrared spectra (IR) were recorded on a JASCO FT/IR4100 spectrometer equipped with a diamond ATR unit. Absorption spectra were recorded on a JASCO V670 spectrophotometer. MALDI-TOF mass spectra were measured on a Bruker Daltonics autoflex III smartbeam with 1,1,4,4-tetraphenylbuta-1,3-diene (TPB) as the matrix. Isotope distribution patterns were simulated using ChemCalc.[1] Electrochemical measurements were performed using an ALS electrochemical analyzer (model 630DT; BAS). Platinum wires were used as the working electrode and the counter electrode. The reference electrode was a saturated calomel reference electrode (SCE). Analytes were dissolved in 1,2-DCB with $(n\text{-Bu})_4NPF_6$ (0.1 M). They were deaerated using freeze–pump–thaw cycles under reduced pressures. The measurement settings were as follows: scan rate = 20 mV s^{-1} for cyclic voltammetry (CV) measurements and pulse amplitude = 50 mV, pulse width = 200 msec, pulse period = 500 msec for differential pulse voltammetry (DPV) measurements. All potentials are referenced to the ferrocene/ferrocenium couple (Fc/Fc^{+}) as the standard.

2-Methylbut-3-yn-2-yl acetate (**1a**), 2-methylbut-3-yn-2-yl benzoate (**1b**), 1,1-diphenylprop-2-ynyl acetate (**1c**), and 1-benzoyloxy-3-methyl-1,2-butadiene (**4**) were prepared according to literature procedures.[2–5] Their NMR data are in accord with the literature values.

2. General procedure for the reaction of C_{60} with 1 (or 4).

A 54 mL aliquot of a 1,2-DCB solution containing C_{60} (54 mg, 0.075 mmol), 3–9 equiv. of **1** (or **4**), and 0.1–0.4 equiv. of a metal catalyst ($PtCl_2$, CuCl, or $AgOCOCF_3$; 5 mol% based on **1** (or **4**)) was placed in a pyrex tube, degassed using freeze–pump–thaw cycles under reduced pressures, and heated at 110–190ºC. Purification and isolation was accomplished by FC followed by preparative HPLC (Buckyprep ϕ20 × 250 mm; Cosmosil; Nacalai Tesque Inc., toluene/*n*-hexane 1:1, flow rate 9.9 mL min^{-1}) to give **2** and **3**.

2a: Brown solid; R_f = 0.16 (SiO_2; toluene/*n*-hexane 1:2). δ_H (400 MHz, $CDCl_3$, r.t.) 2.19 (3H, d, *J* 0.9, 3H; C=C(C*H*$_3$)), 2.35 (3H, s; -COC*H*$_3$), 2.40 (3H, d, *J* 1.4; C=C(C*H*$_3$)), 7.03–7.06 (1H, m; C*H*) ppm; δ_C (100 MHz, $CDCl_3$, r.t.) 20.66 (C65 or C64), 20.85 (C67), 21.12 (C64 or C65), 72.41 (C1), 73.17 (C2), 77.71 (C61), 127.63, 130.31, 130.50 (C62), 137.42, 137.59, 137.66, 139.42, 140.34, 140.48, 140.60, 140.65 (C63), 141.43, 141.89, 141.96, 142.00, 142.22, 142.24, 142.28, 142.39, 142.41, 142.49, 142.53, 142.66, 142.72, 142.77, 142.85, 142.90, 144.32, 144.37, 144.46, 144.56, 145.15, 145.18, 145.22, 145.28, 145.32, 145.36, 145.48, 145.94, 146.00, 146.06, 146.27, 146.36, 146.81, 146.86, 147.67, 148.55, 151.15, 151.93, 152.38, 170.66 (C66) ppm (48 resonances out of 58 expected ones due to peak overlap for the cage carbon atoms); λ_{max} (ε) 434 nm (2700 M^{-1} cm^{-1}); ν_{max}(ATR)/cm^{-1} 524, 697, 796, 1015, 1211, 1259, 1363, 1424, 1461, 1505, 1738, 2849, 2919, 2957; MALDI-TOF-MS (matrix = TPB, negative mode) *m*/*z* 845.90 ([*M*]$^-$; calcd for $C_{67}H_{10}O_2$, 846.07), 719.97 ([*M* – $C_7H_{10}O_2$]$^-$; calcd for C_{60}, 720.00).

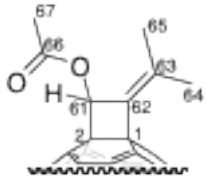

2a

3a: Brown solid; R_f = 0.16 (SiO_2; toluene/*n*-hexane 1:2); δ_H (400 MHz, $CDCl_3$/CS_2 1:1, 318 K) 2.28 (3H, s; -COC*H*$_3$), 2.36–2.37 (3H, m; C=C(C*H*$_3$)), 4.03 (1H, brd, *J* 14.0; C*H*$_2$), 4.26 (1H, brd, *J* 14.0; C*H*$_2$), 6.58 (1H, d, *J* 3.9, 1H; C=C*H*), 6.90 (1H, dd, 3.9, 1.4; -C*H*(OCOCH$_3$)) ppm; δ_C (100 MHz, $CDCl_3$/CS_2 1:1, r.t.) δ 20.95 (C67), 23.64 (C65), 44.42 (C62), 64.69 (C2), 69.12 (C1), 74.81 (C61), 125.68 (C63), 135.25, 135.69, 136.25, 136.62, 139.39, 139.77, 140.19, 140.26, 141.41, 141.49, 141.59, 141.91, 141.94, 141.97, 142.00, 142.11, 142.14 (C64), 142.58, 142.52, 143.03, 143.06, 144.54, 144.58, 144.62, 144.96, 145.08, 145.36, 145.41, 145.51, 145.62, 145.67, 146.08, 146.14, 146.20, 146.47, 147.49, 147.54, 153.07, 156.59, 156.68, 169.54 (C66) ppm (39 resonances out of 58 expected ones due to peak overlap for the cage carbon atoms); λ_{max} (ε) 434 nm (3100 M^{-1} cm^{-1}); ν_{max}(ATR)/cm^{-1} 524, 696, 745, 793, 1015, 1081, 1207, 1258, 1364, 1425, 1364, 1425, 1509, 1738, 2845, 2916,

2961; MALDI-TOF-MS (matrix = TPB, negative mode) *m*/*z* 845.90 ([*M*]$^-$; calcd for $C_{67}H_{10}O_2$, 846.07), 786.02 ([*M* – $C_2H_4O_2$]$^-$; calcd for $C_{65}H_6$, 786.05), 719.99 ([*M* – $C_7H_{10}O_2$]$^-$; calcd for C_{60}, 720.00).

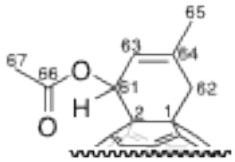

3a

2b: Brown solid; R_f = 0.53 (SiO_2; toluene/*n*-hexane 1:1); δ_H (400 MHz, $CDCl_3/CS_2$ 1:2, r.t.) δ 2.25 (3H, d, *J* 0.92; C=C(C*H*$_3$)), 2.45 (3H, d, *J* 1.4; C=C(C*H*$_3$)), 7.28–7.30 (1H, m; C*H*), 7.51–7.52 (2H, m; Ph-H_{meta}), 7.63–7.67 (1H, m; Ph-H_{para}), 8.25–8.28 (2H, m; Ph-H_{ortho}) ppm; δ_C (100 MHz, $CDCl_3/CS_2$ 1:2, r.t.) δ 20.72 (C64 or C65), 21.23 (C65 or C64), 72.60 (C1), 73.45 (C2), 78.25 (C61), 128.68 (C69), 129.50, 130.14 (C68), 130.69 (C62 or C63), 133.58 (C70), 137.52, 137.75, 139.38, 140.45, 140.56, 140.69, 140.77 (C63 or C62), 141.56, 141.97, 142.01, 142.06, 142.27, 142.31, 142.35, 142.49, 142.56, 142.62, 142.71, 142.77, 142.82, 142.87, 142.97, 144.37, 144.43, 144.51, 144.65, 145.21, 145.24, 145.27, 145.34, 145.41, 145.44, 145.47, 145.53, 145.96, 146.00, 146.07, 146.37, 146.51, 146.87, 146.91, 147.79, 148.76, 151.25, 152.04, 152.53 (C67), 166.30 (C66) ppm (45 resonances out of 58 expected ones due to peak overlap for the cage carbon atoms); λ_{max} (ε) 433 nm (3400 M^{-1} cm^{-1}); ν_{max}(ATR)/cm^{-1} 523, 705, 796, 1024, 1065, 1083, 1257, 1426, 1717, 2847, 2915; MALDI-TOF-MS (matrix = TPB, negative mode) *m*/*z* 907.85 ([*M*]$^-$; calcd for $C_{72}H_{12}O_2$, 908.08), 719.89 ([*M* – $C_{12}H_{12}O_2$]$^-$; calcd for C_{60}, 720.00).

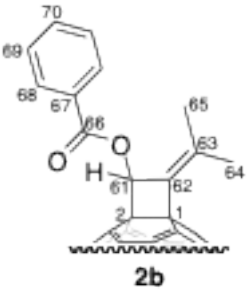

2b

3b: Brown solid; R_f = 0.38 (SiO_2; toluene/*n*-hexane 1:1); δ_H (400 MHz, $CDCl_3/CS_2$ 1:2, r.t.) δ 2.40–2.41 (3H, m; C*H*$_3$), 4.04–4.11 (1H, m; C*H*$_2$), 4.30–4.50 (1H, m; C*H*$_2$), 6.70–6.76 (1H, m; C=C*H*), 7.03–7.04 (1H, m; -C*H*(OCOCH$_3$)), 7.45–7.50 (2H, m; Ph-H_{meta}), 7.58–7.62 (1H, m; Ph-H_{para}), 8.18–8.21 (2H, m; Ph-H_{ortho}) ppm; δ_C (100 MHz, $CDCl_3/CS_2$ 1:2, r.t.) δ 24.01 (C65), 44.59 (C62), 64.66 (C2), 69.22 (C1), 75.64 (C61), 125.68 (C63), 128.59 (C69), 129.82, 129.90 (C68), 133.29 (C70), 135.30, 135.64, 136.48, 136.65, 139.59, 139.87, 140.27, 140.34, 141.49, 141.60, 141.63, 142.03 (C64), 142.11, 142.17, 142.27, 142.54, 142.60, 142.63, 143.10, 144.60, 144.65, 144.69, 145.00, 145.22, 145.41, 145.46, 145.57, 145.71, 145.73, 146.20, 146.23, 146.51, 147.60, 153.26

(C67 or cage carbon), 153.36 (cage carbon or C67), 156.71, 156.95, 165.27 (C66) ppm (36 resonances out of 58 expected ones due to peak overlap for the cage carbon atoms); λ_{max} (ε) 434 nm (3200 M^{-1} cm^{-1}); ν_{max}(ATR)/cm^{-1} 524, 703, 774, 794, 1023, 1064, 1083, 1173, 1257, 1427, 1508, 1716, 2848, 2920, 2955; MALDI-TOF-MS (matrix = TPB, negative mode) *m*/*z* 908.06 ([*M*]$^-$; calcd for $C_{72}H_{12}O_2$, 908.08), 786.01 ([*M* – $C_7H_6O_2$]$^-$; calcd for $C_{65}H_6$, 786.05), 719.94 ([*M* – $C_{12}H_{12}O_2$]$^-$; calcd for C_{60}, 720.00).

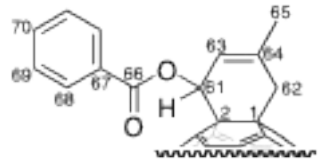

3b

2c: Brown solid; R_f = 0.33 (SiO_2; toluene/*n*-hexane 1:1), δ_H (400 MHz, CD_2Cl_2 /CS_2 3:1, r.t.) δ = 2.22 (3H, s; -COC*H*$_3$), 7.20–7.24 (1H, m; Ph-H_{para}), 7.26–7.30 (2H, m; Ph-H_{meta}), 7.41–7.46 (1H, m; Ph-H_{para}), 7.47 (1H, s; C*H*), 7.48–7.52 (2H, m; Ph-H_{meta}), 7.56–7.58 (2H, m; Ph-H_{ortho}), 7.68–7.71 (2H, m; Ph-H_{ortho}) ppm; δ_C (100 MHz, CD_2Cl_2 /CS_2 3:1, r.t.) δ = 20.96 (C73), 73.72 (C1), 74.07 (C2), 78.40 (C61), 128.67 (CH), 128.85 (CH), 128.94 (CH), 128.95 (CH), 128.96 (CH), 130.39 (CH), 136.85, 137.08 (C62 or C63), 137.45 (C63 or C62), 138.11, 138.49 (C64 or C68), 139.64 (C68 or C64), 139.84, 139.95, 139.98, 140.76, 141.00, 141.95, 142.32, 142.44, 142.49, 142.59, 142.67, 142.69, 143.02, 143.09, 143.12, 143.16, 143.19, 144.73, 144.77, 144.80, 144.89, 145.42, 145.57, 145.60, 145.64, 145.71, 145.77, 145.81, 145.83, 145.94, 146.34, 146.38, 146.43, 146.51, 146.58, 146.71, 146.92, 147.28, 147.30, 147.97, 148.02, 149.00, 152.20, 152.57, 152.78, 170.59 (C72) ppm (47 resonances out of 58 expected ones due to peak overlap for the quaternary cage carbon atoms); λ_{max} (ε) 434 nm (1800 M^{-1} cm^{-1}); ν_{max}(ATR)/cm^{-1} 523, 695, 727, 762, 799, 1019, 1068, 1096, 1124, 1208, 1259, 1366, 1423, 1441, 1461, 1493, 1741, 2850, 2920, 2953; MALDI-TOF-MS (matrix = TPB, negative mode) *m*/*z* 969.98 ([*M*]$^-$; calcd for $C_{77}H_{14}O_2$, 970.10), 719.94 ([*M* – $C_{17}H_{14}O_2$]$^-$; calcd for C_{60}, 720.00).

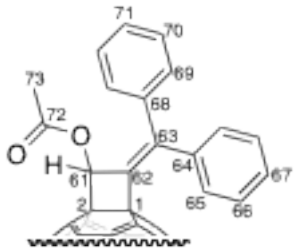

2c

Calculations

DFT calculations were performed using *Gaussian 09* (Rev. D.01)[6] at the B3LYP/6–31G(d)[7] level of theory. Before structure optimization, the CONFLEX conformational search procedure was used to find low-energy conformations using *CONFLEX7*.[8] Calculations of NMR spectra were performed at the GIAO-B3LYP/6–31G(d) level of theory using the B3LYP/6–31G(d) optimized geometries. We calculated ^{1}H and ^{13}C NMR spectra of a Bingel-Hirsch type cyclopropanated adduct, C_{60}(CHPh), as a model to assess validity of the basis sets and the functional, and found that the calculated spectra were in good agreement with the reported experimental data (see Figure S33).[9] Therefore, we concluded that our calculations performed at the B3LYP/6–31G(d) level of theory were sufficient for the simulation of NMR data of the fullerene derivatives presented.

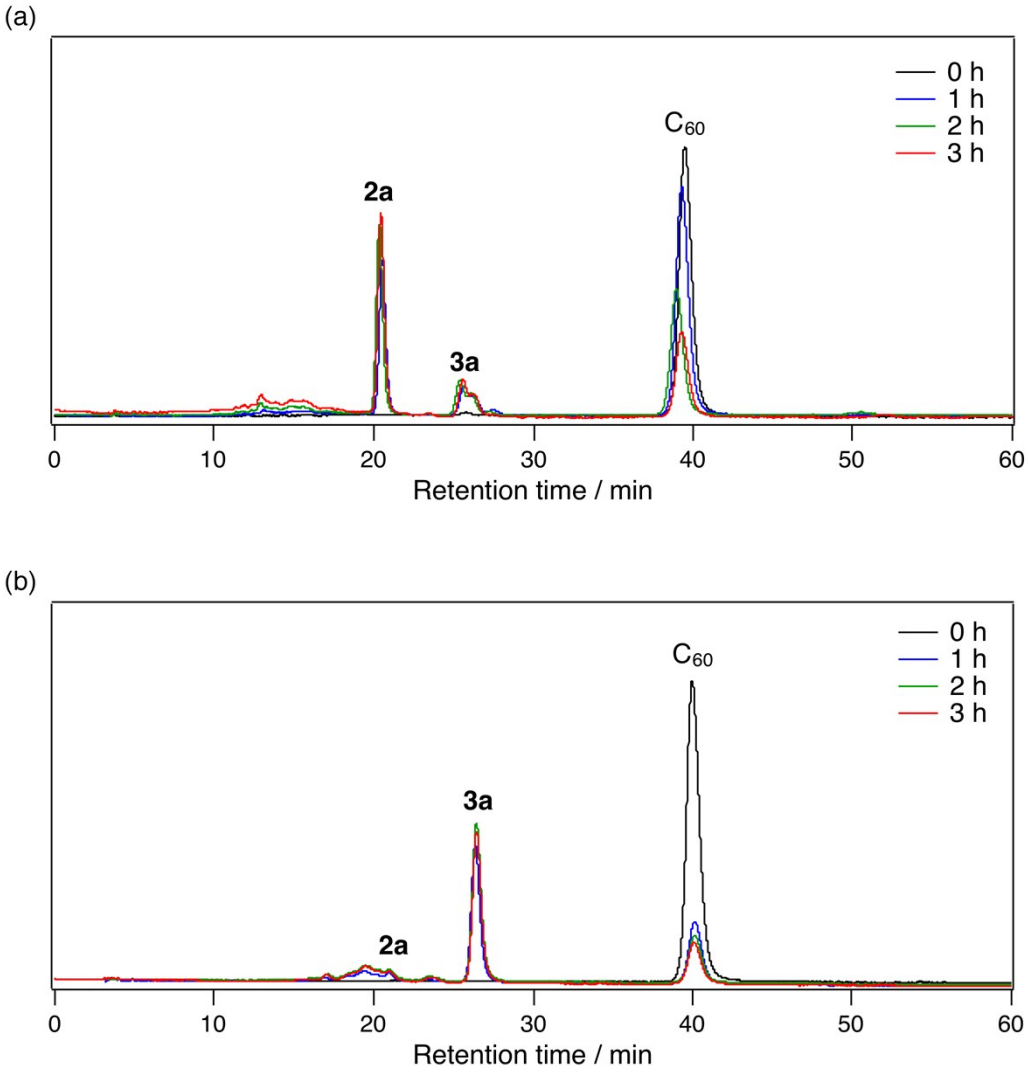

Fig. S1. Two contrasting HPLC profiles of the reaction mixtures in the reaction of C_{60} with **1a** in the presence of metal catalyst; (a) entry 3 in Table 1 (metal catalyst, CuCl), and (b) entry 4 in Table 1 (metal catalyst, $AgOCOCF_3$). Conditions: Buckyprep column (4.6 mm × 250 mm i.d.); column temp., 40ºC; flow rate, 1 mL min^{-1}; eluent, toluene/*n*-hexane 1:2.

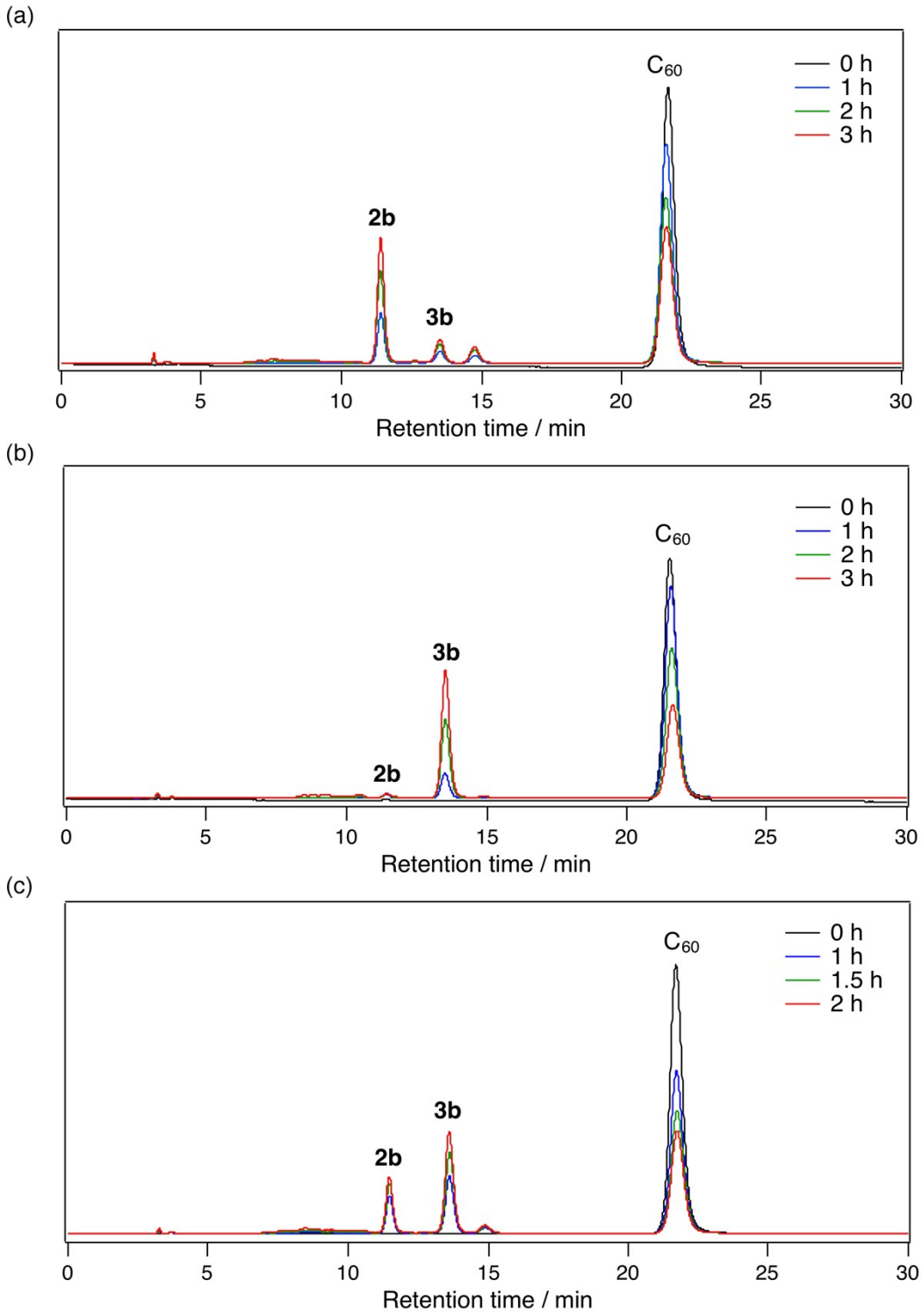

Fig. S2. Three contrasting HPLC profiles of the reaction mixtures in the reaction of C_{60} with **4** in the presence or absence of metal catalyst; (a) entry 1 in Table 2 (metal catalyst, CuCl), (b) entry 2 in Table 2 (metal catalyst, $AgOCOCF_3$), and entry 3 in Table 2 (metal catalyst, none). Conditions: Buckyprep column (4.6 mm × 250 mm i.d.); column temp., 40ºC; flow rate, 1 mL min^{-1}; eluent, toluene/*n*-hexane 1:1.

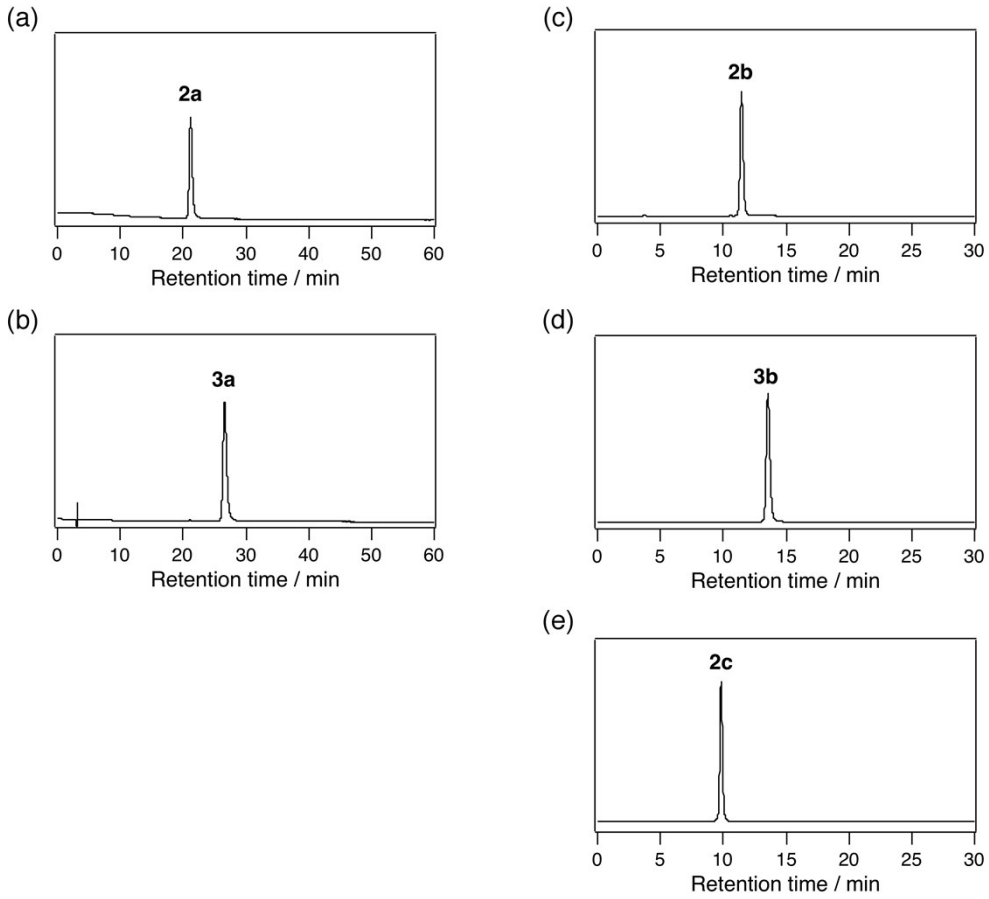

Fig. S3. HPLC profiles of (a) **2a**, (b) **3a**, (c) **2b**, (d) **3b**, and (e) **2c**. Conditions: Buckyprep column (4.6 mm × 250 mm i.d.); column temp., 40ºC; flow rate, 1 mL min^{-1}; eluent, toluene/*n*-hexane 1:2 for **2a** and **3a**, toluene/*n*-hexane 1:1 for **2b**, **3b**, and **2c**.

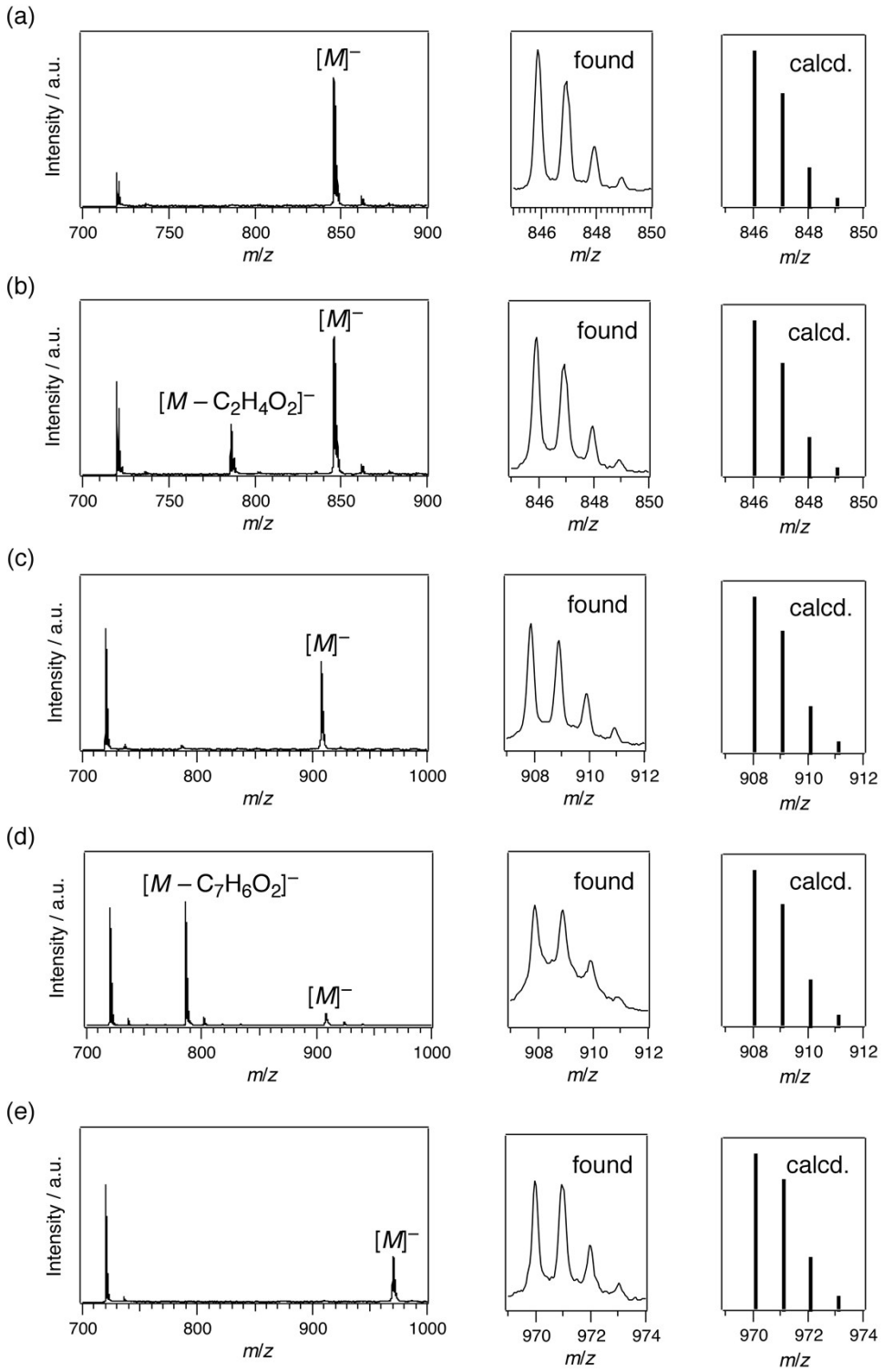

Fig. S4. Negative-mode MALDI-TOF mass spectra of (a) **2a**, (b) **3a**, (c) **2b**, (d) **3b**, and (e) **2c**. Matrix = 1,1,4,4-tetraphenyl-1,3-butadiene (TPB).

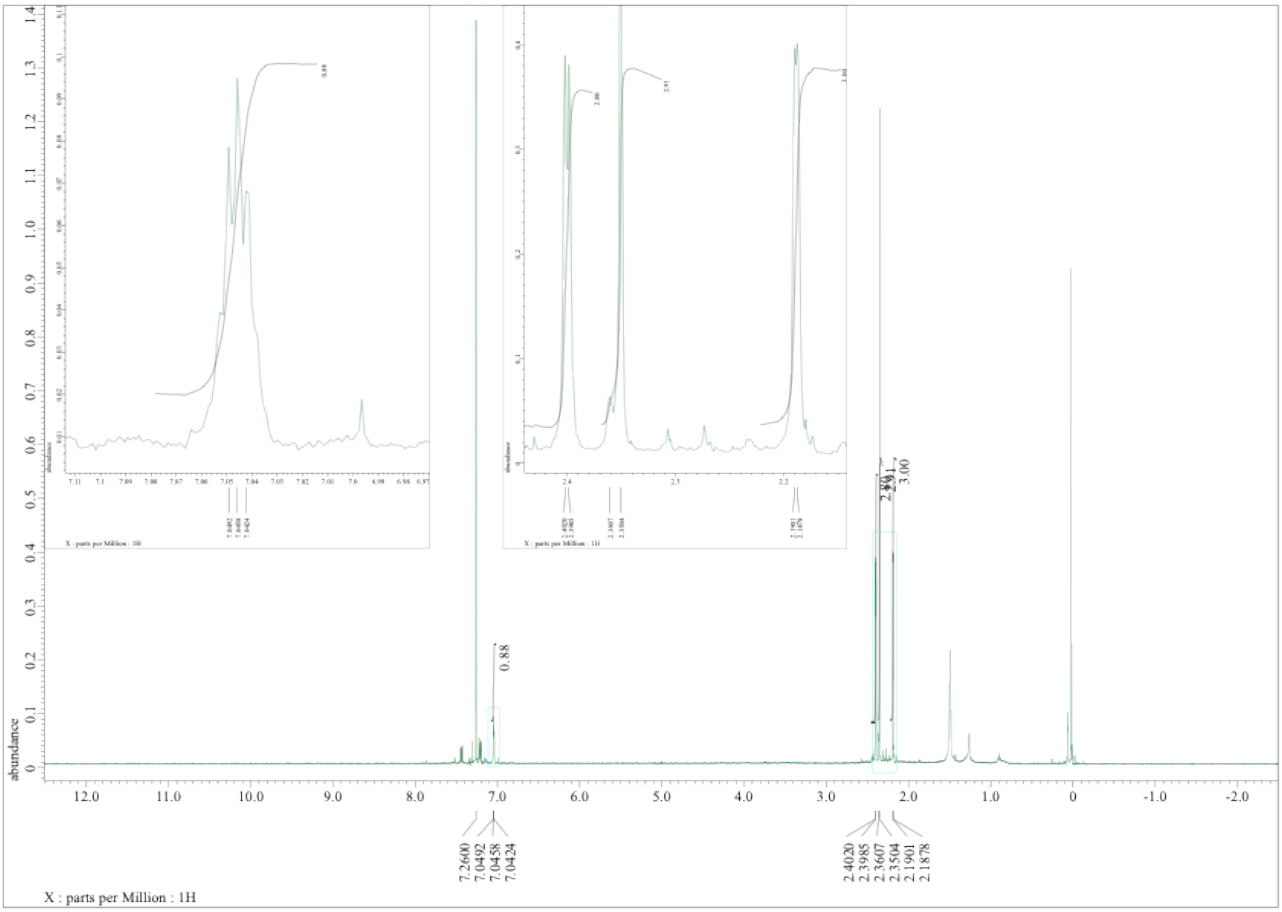

Fig. S5. ^{1}H NMR spectrum of **2a** recorded in $CDCl_3$.

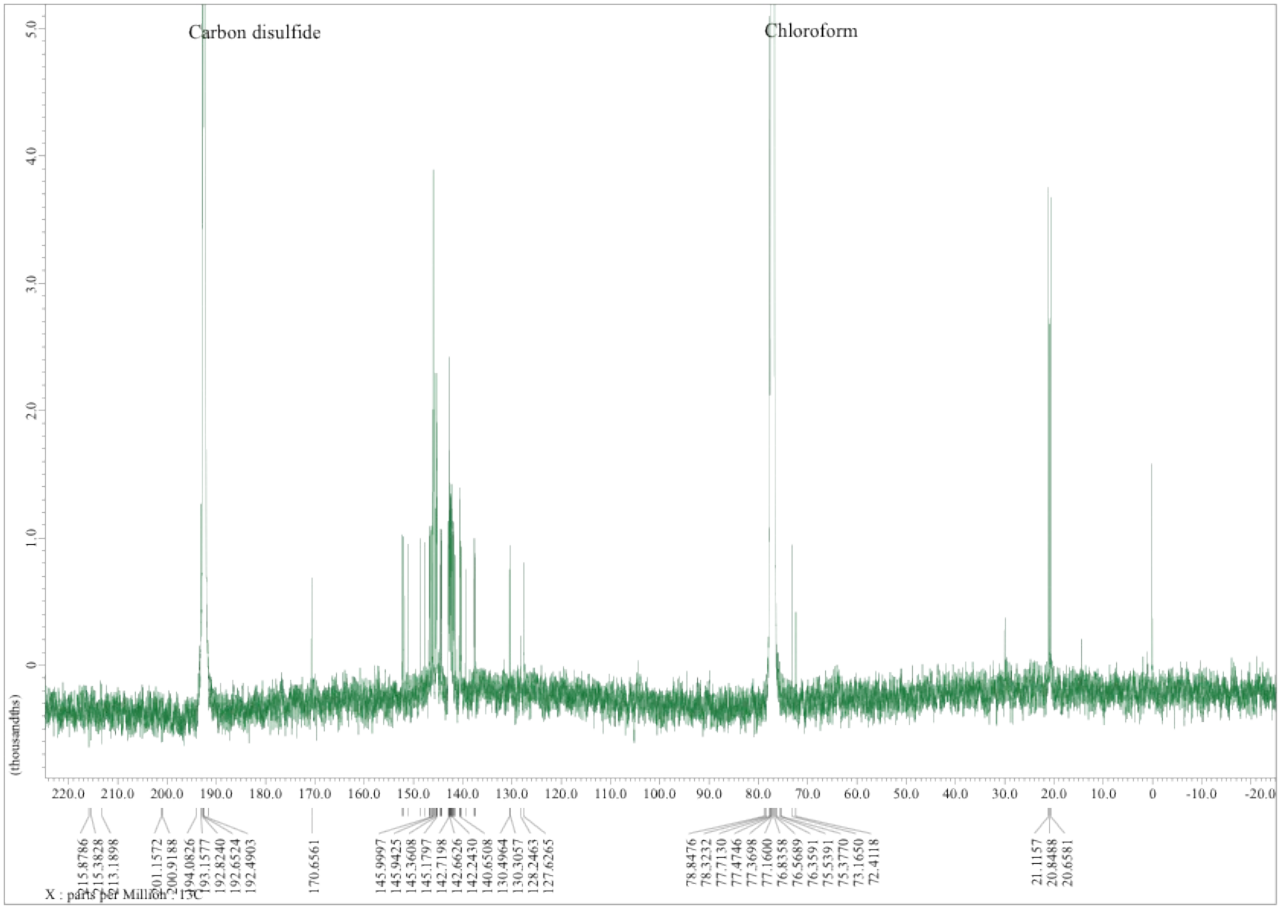

Fig. S6. ^{13}C NMR spectrum of **2a** recorded in $CDCl_3$.

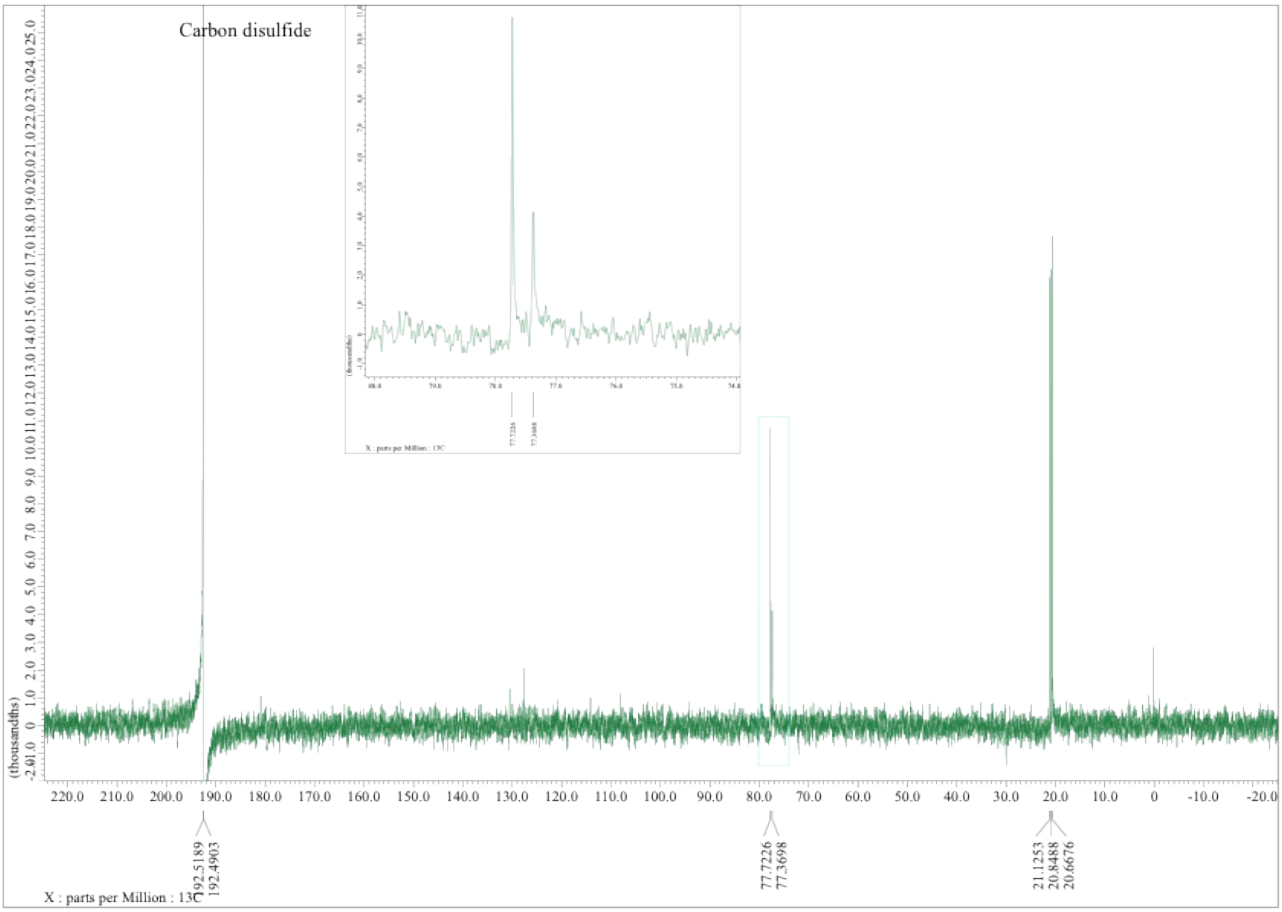

Fig. S7. Dept-135 NMR spectrum of **2a** recorded in $CDCl_3$.

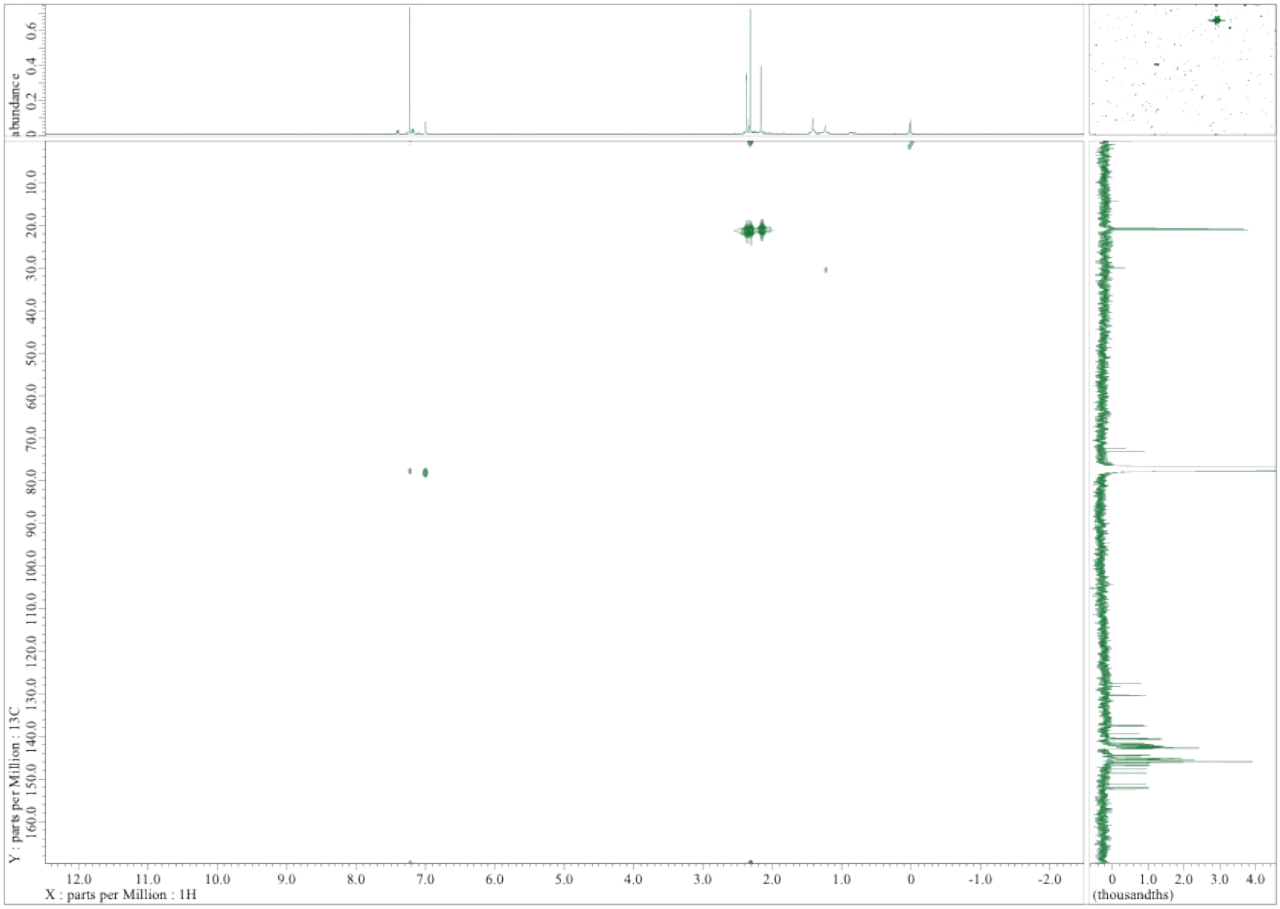

Fig. S8. HMQC NMR spectrum of **2a** recorded in $CDCl_3$.

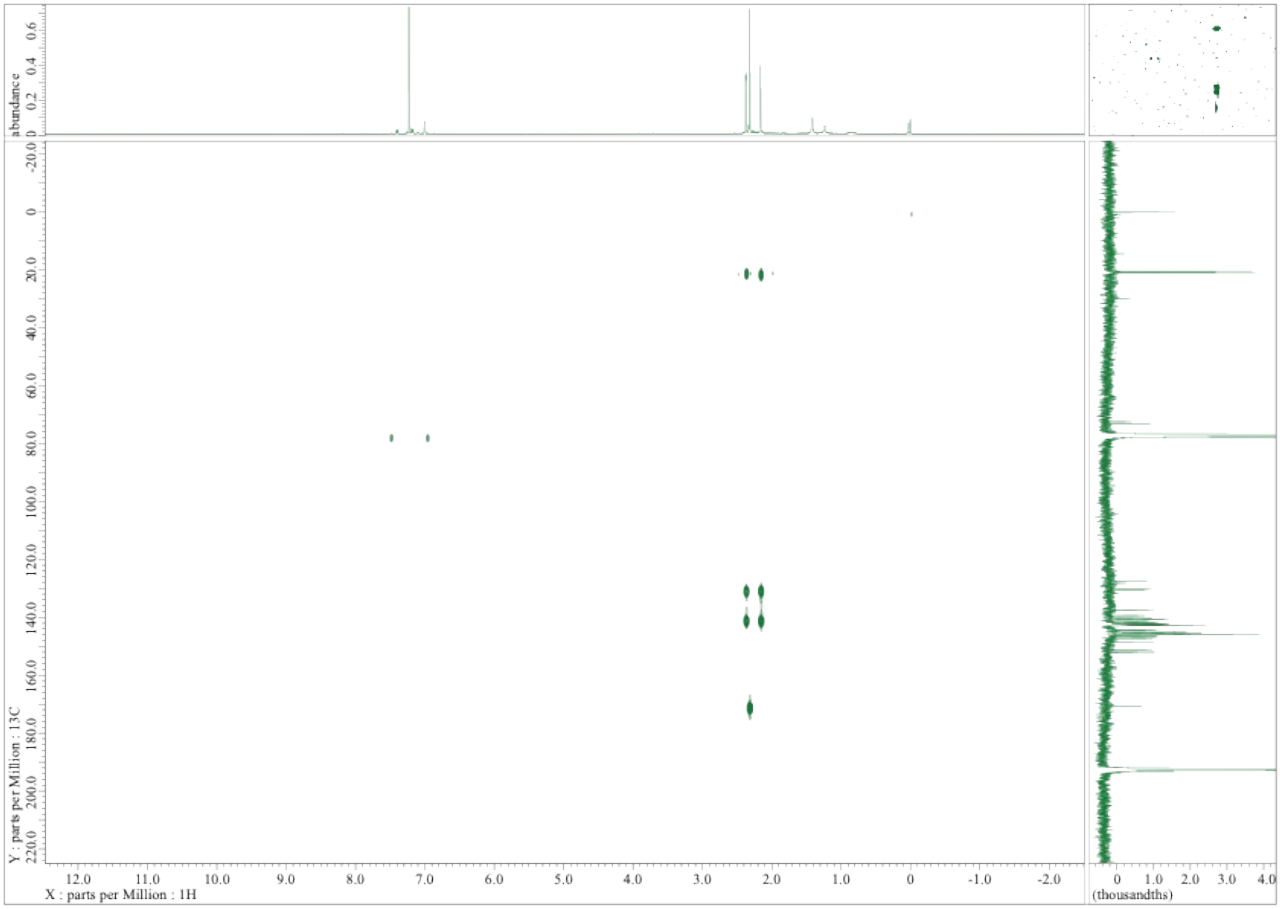

Fig. S9. HMBC NMR spectrum of **2a** recorded in $CDCl_3$.

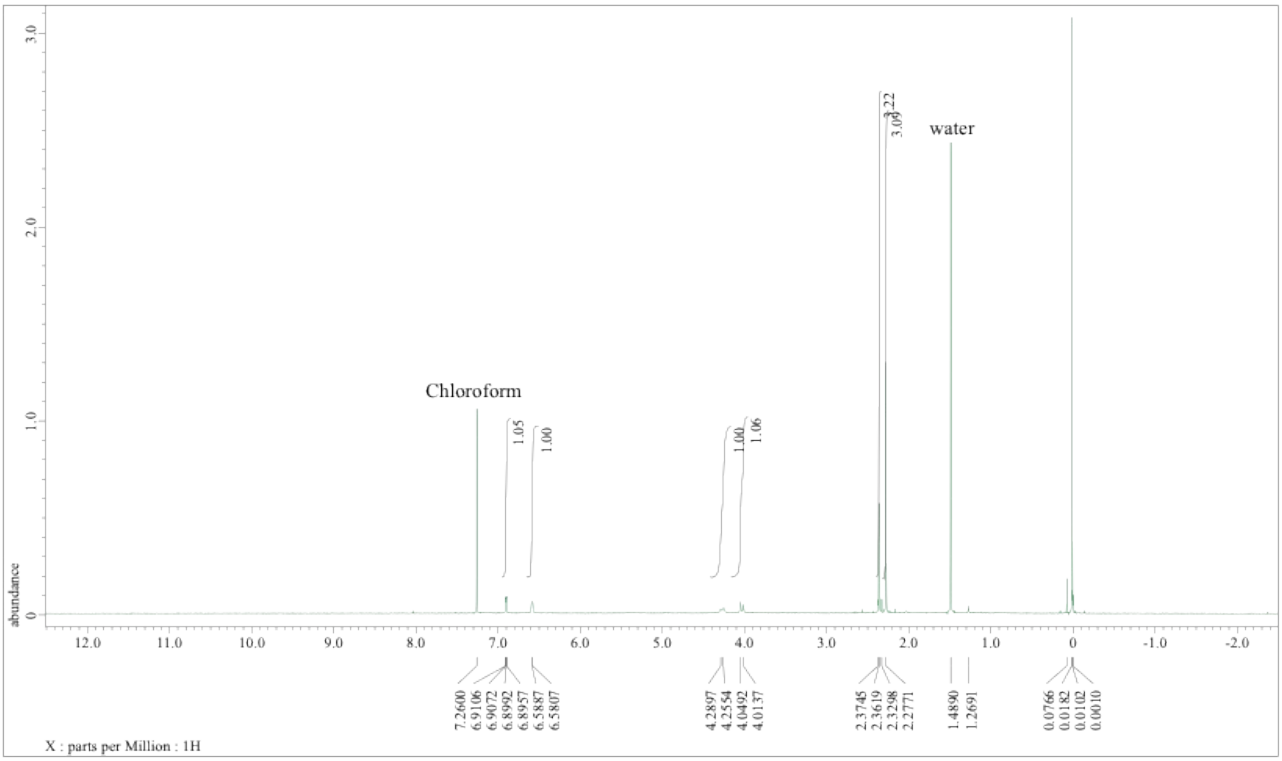

Fig. S10. ^{1}H NMR spectrum of **3a** recorded in $CDCl_3/CS_2$ (1:1) at 318 K.

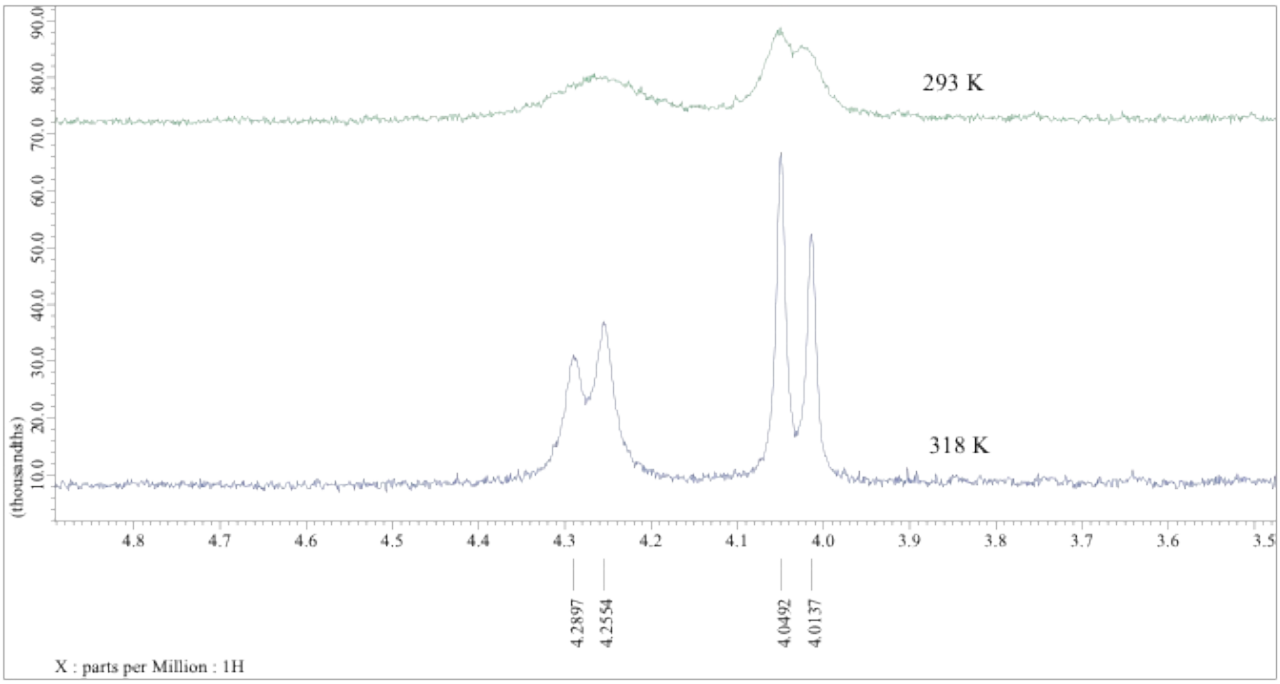

Fig. S11. Variable-temperature ^{1}H NMR spectrum of **3a** recorded in $CDCl_3$ (expanded view).

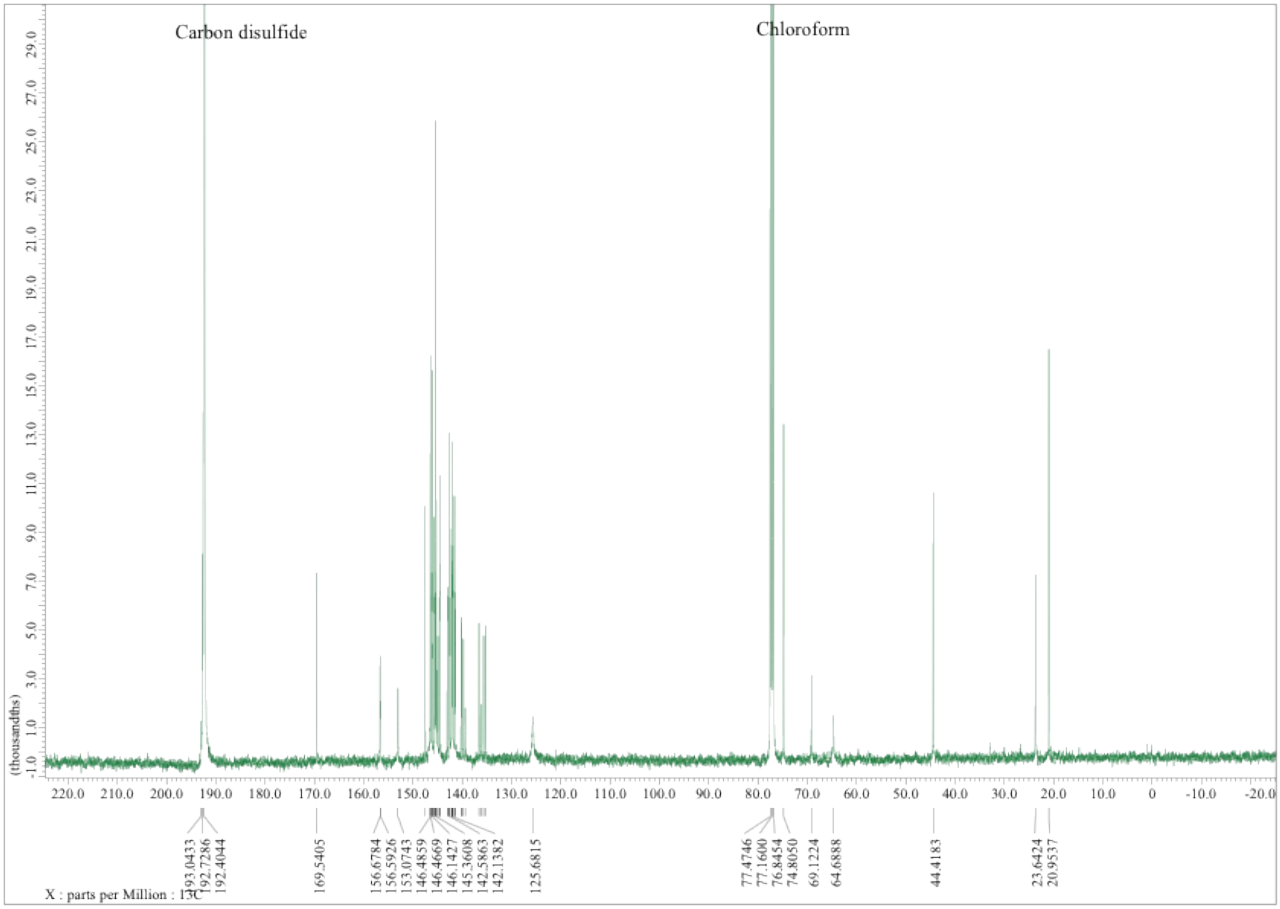

Fig. S12. ^{13}C NMR spectrum of **3a** recorded in $CDCl_3/CS_2$ (1:1).

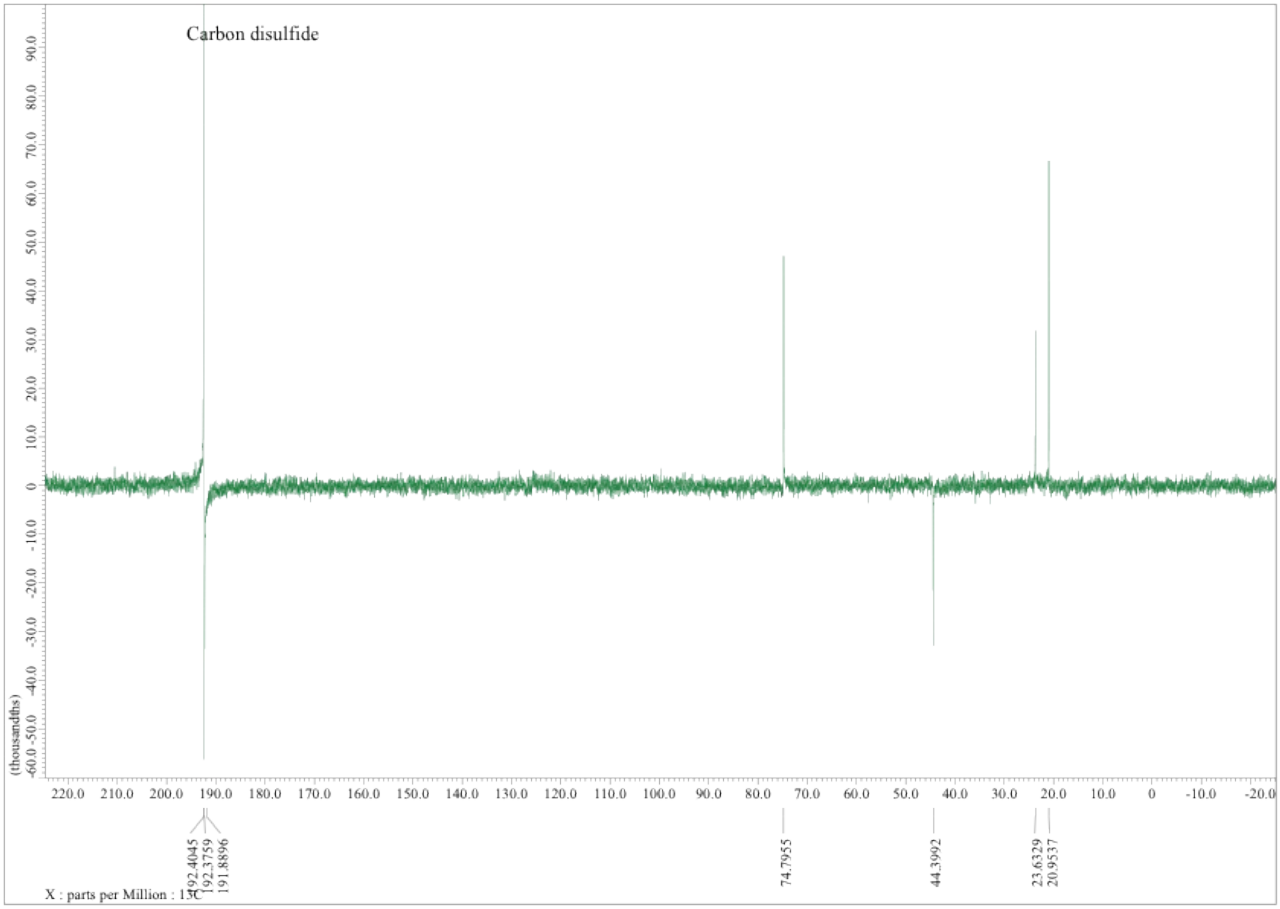

Fig. S13. Dept-135 NMR spectrum of **3a** recorded in $CDCl_3/CS_2$ (1:1).

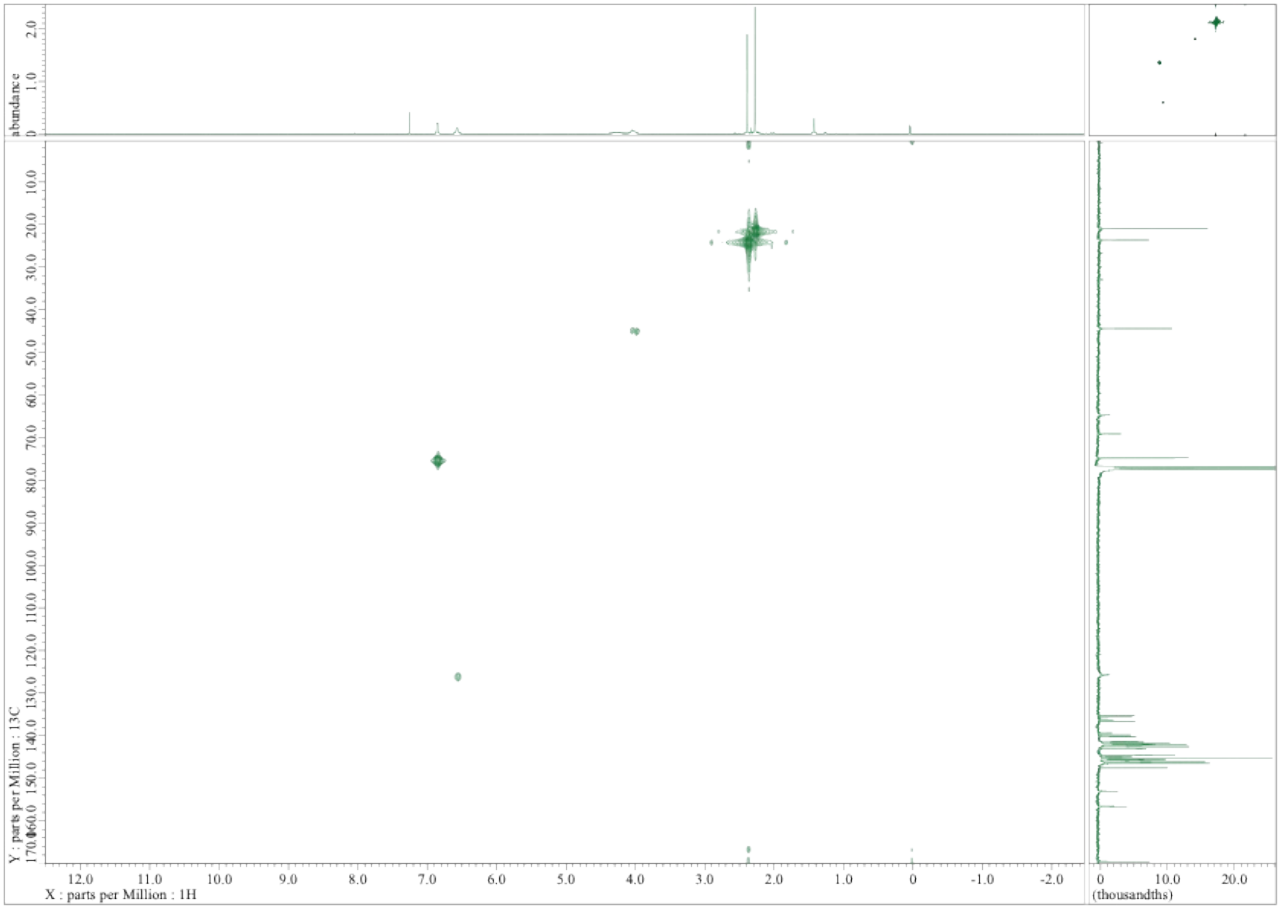

Fig. S14. HMQC NMR spectrum of **3a** recorded in $CDCl_3/CS_2$ (1:1).

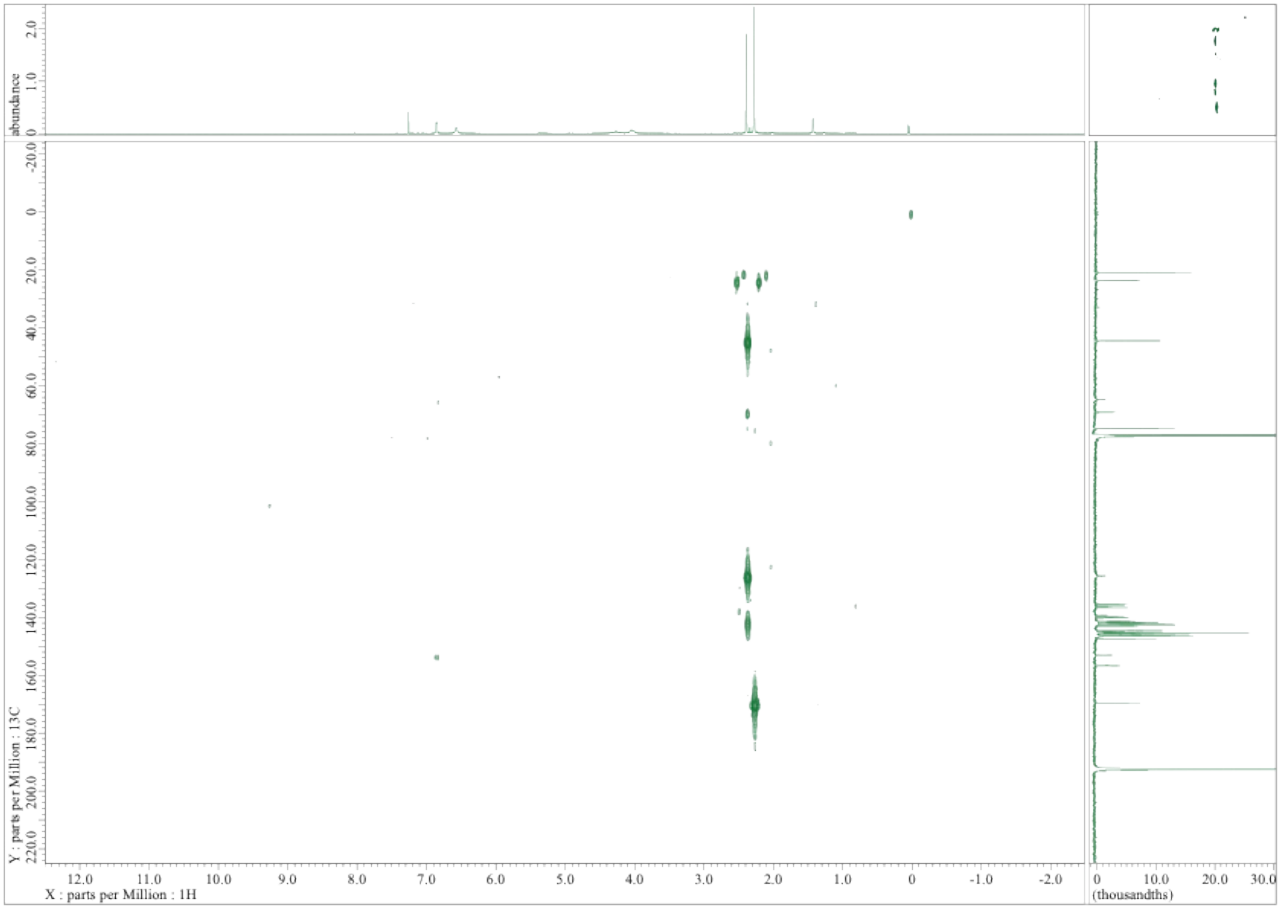

Fig. S15. HMBC NMR spectrum of **3a** recorded in $CDCl_3/CS_2$ (1:1).

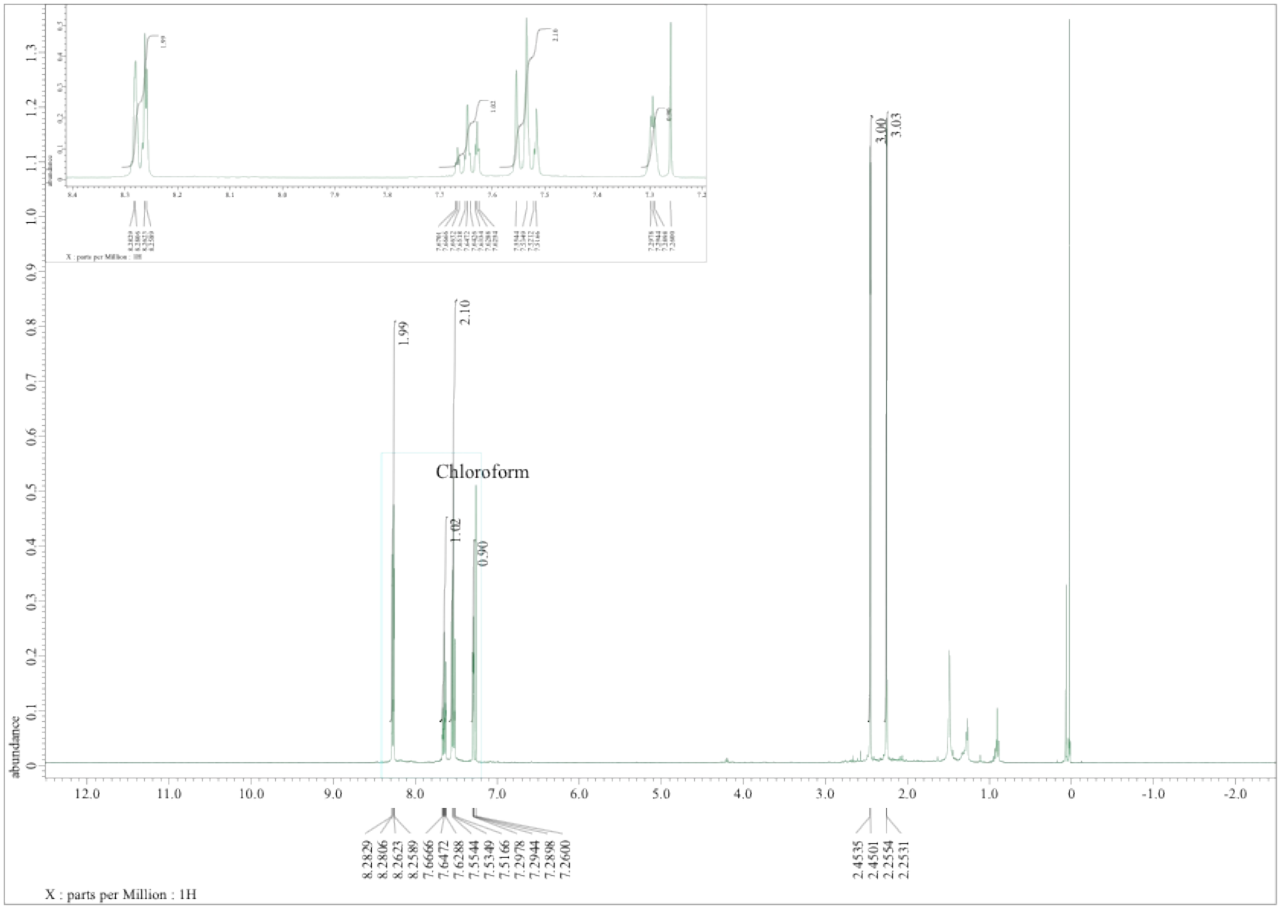

Fig. S16. ^{1}H NMR spectrum of **2b** recorded in $CDCl_3/CS_2$ (1:2).

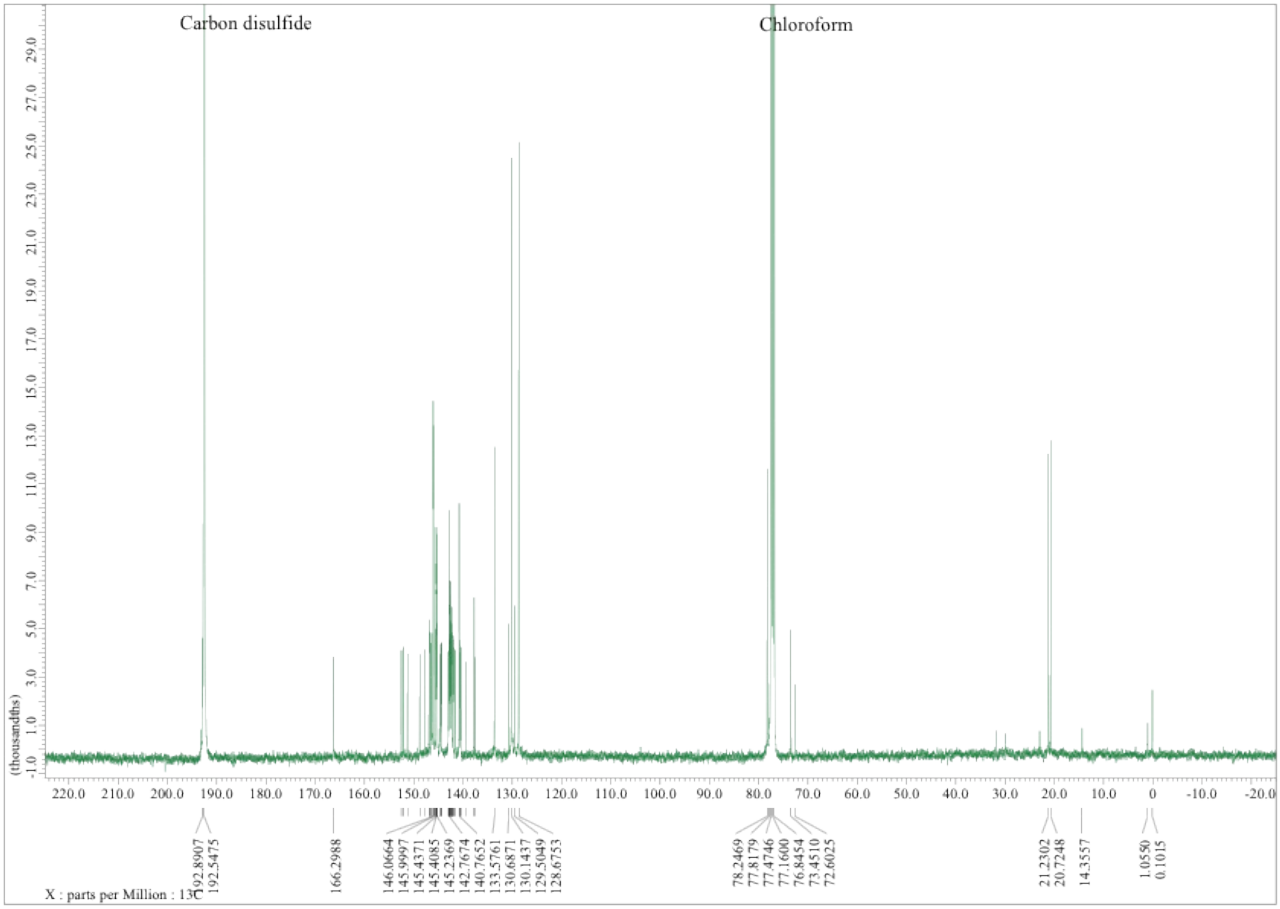

Fig. S17. ^{13}C NMR spectrum of **2b** recorded in $CDCl_3/CS_2$ (1:2).

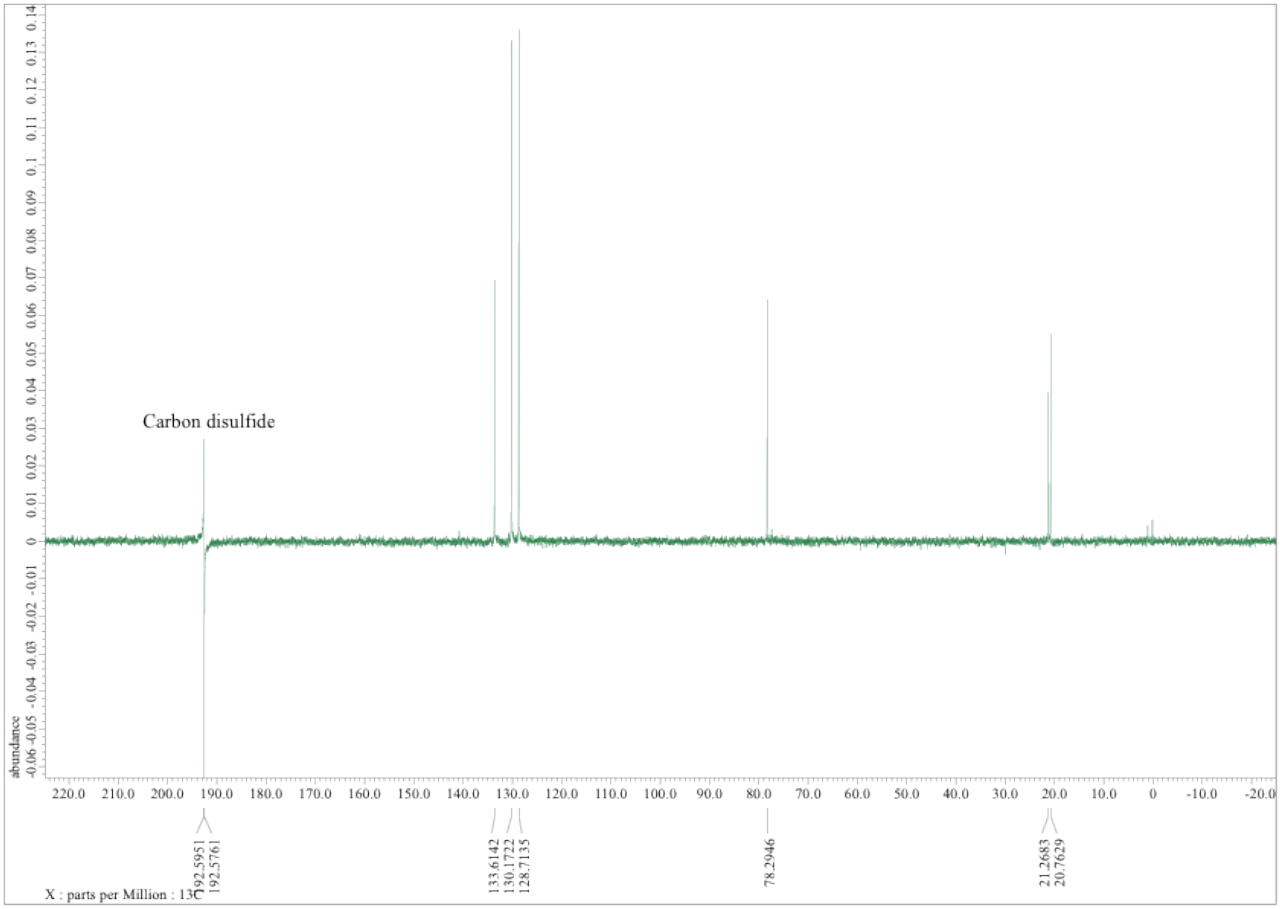

Fig. S18. Dept-135 NMR spectrum of **2b** recorded in $CDCl_3/CS_2$ (1:2).

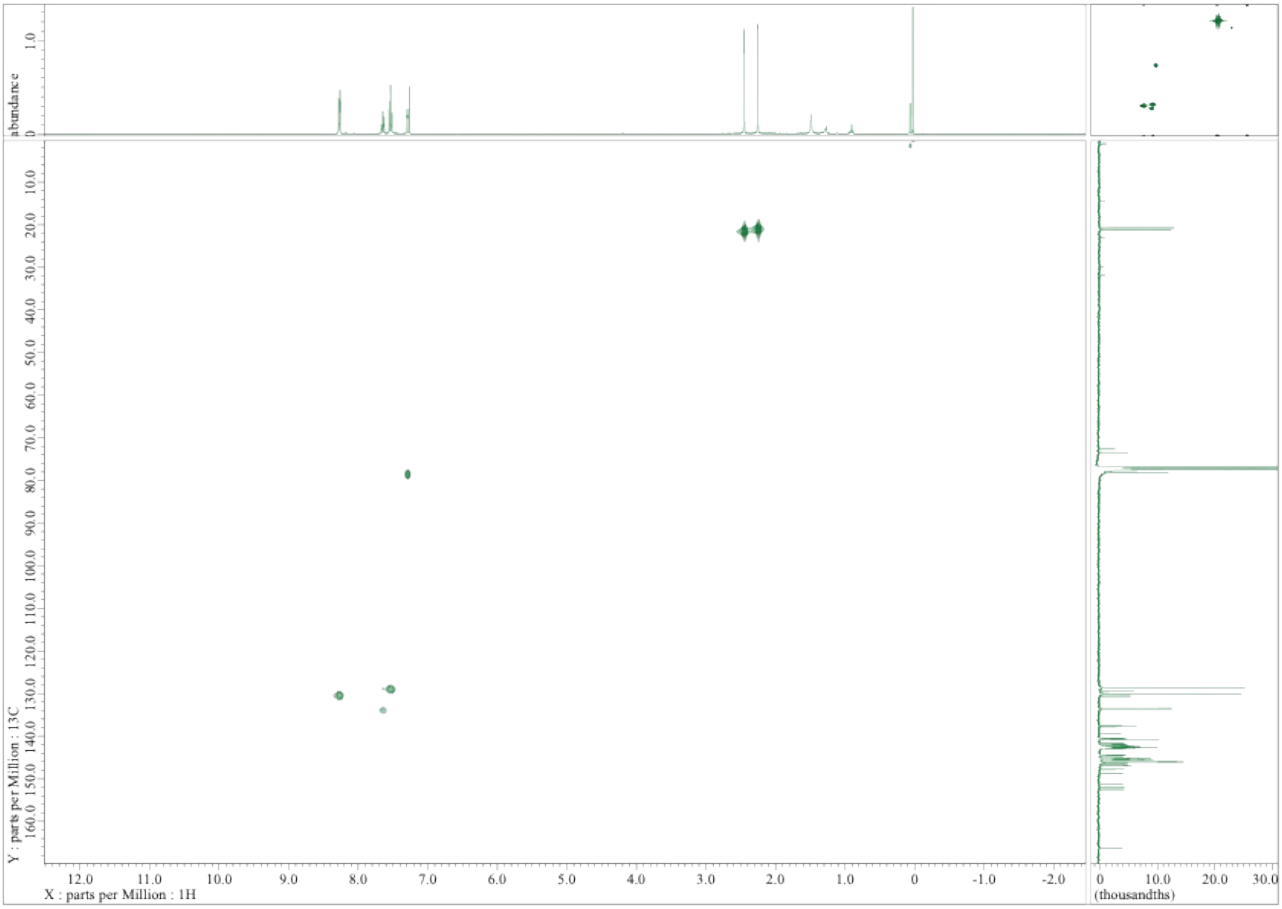

Fig. S19. HMQC NMR spectrum of **2b** recorded in $CDCl_3/CS_2$ (1:2).

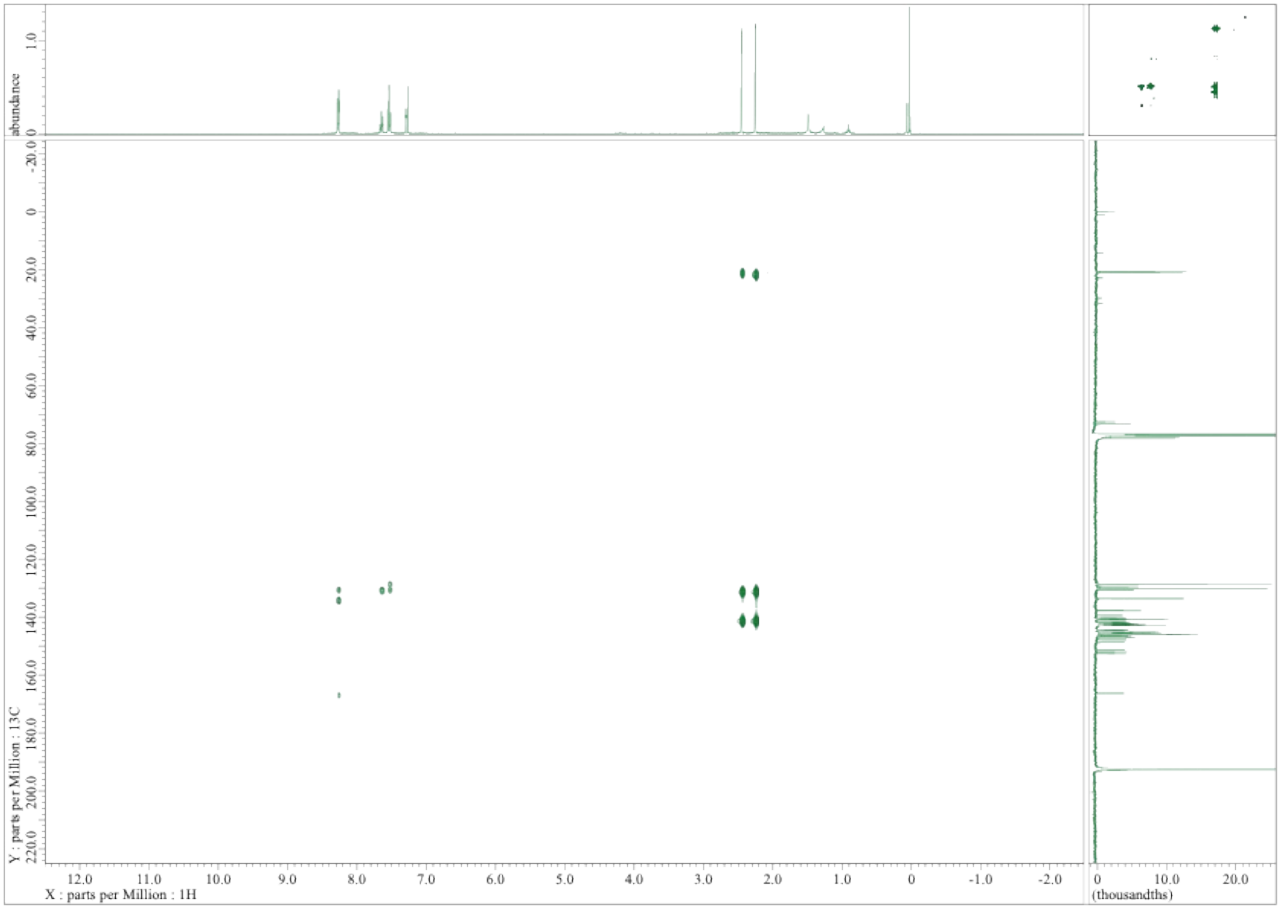

Fig. S20. HMBC NMR spectrum of **2b** recorded in $CDCl_3/CS_2$ (1:2).

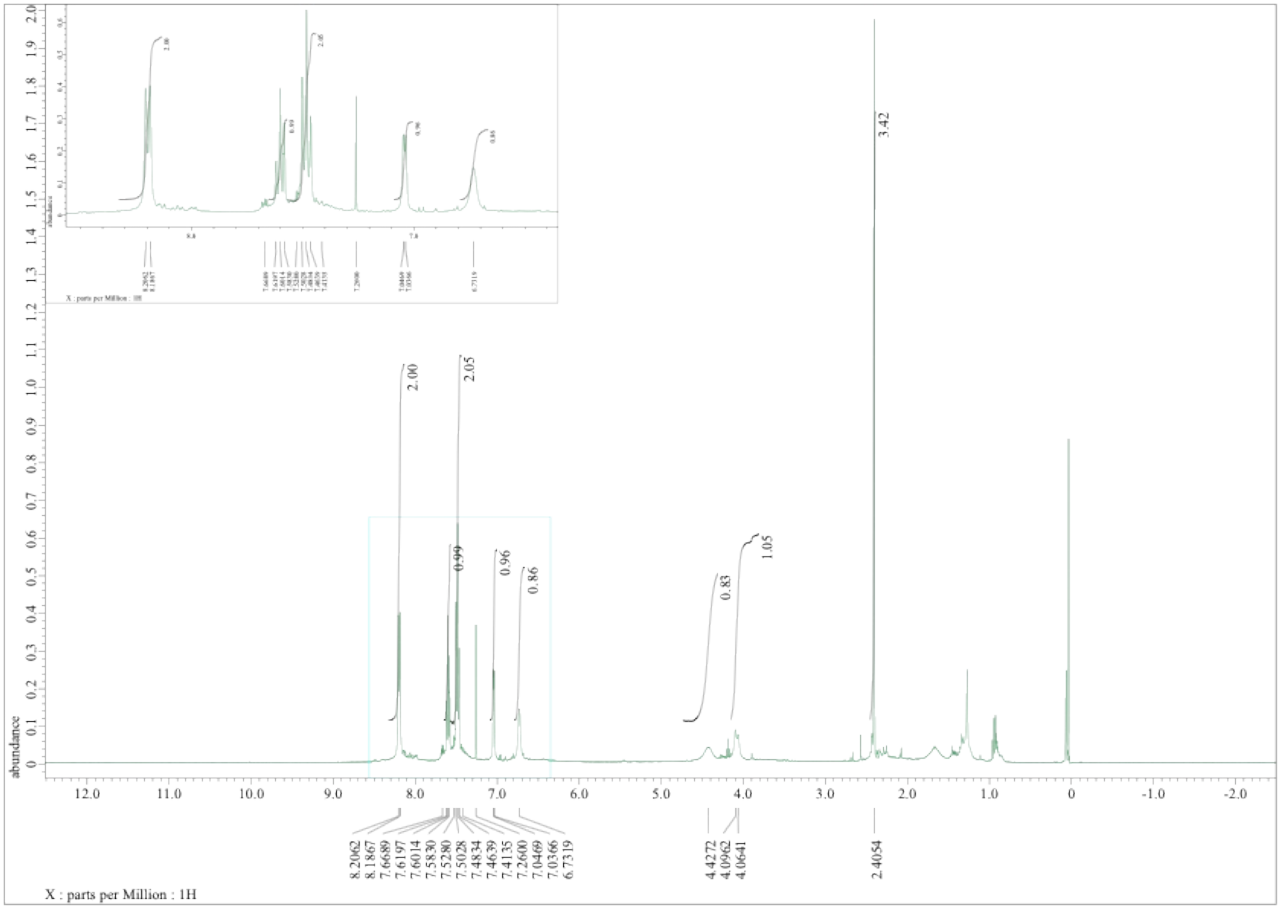

Fig. S21. ^{1}H NMR spectrum of **3b** recorded in $CDCl_3/CS_2$ (1:2).

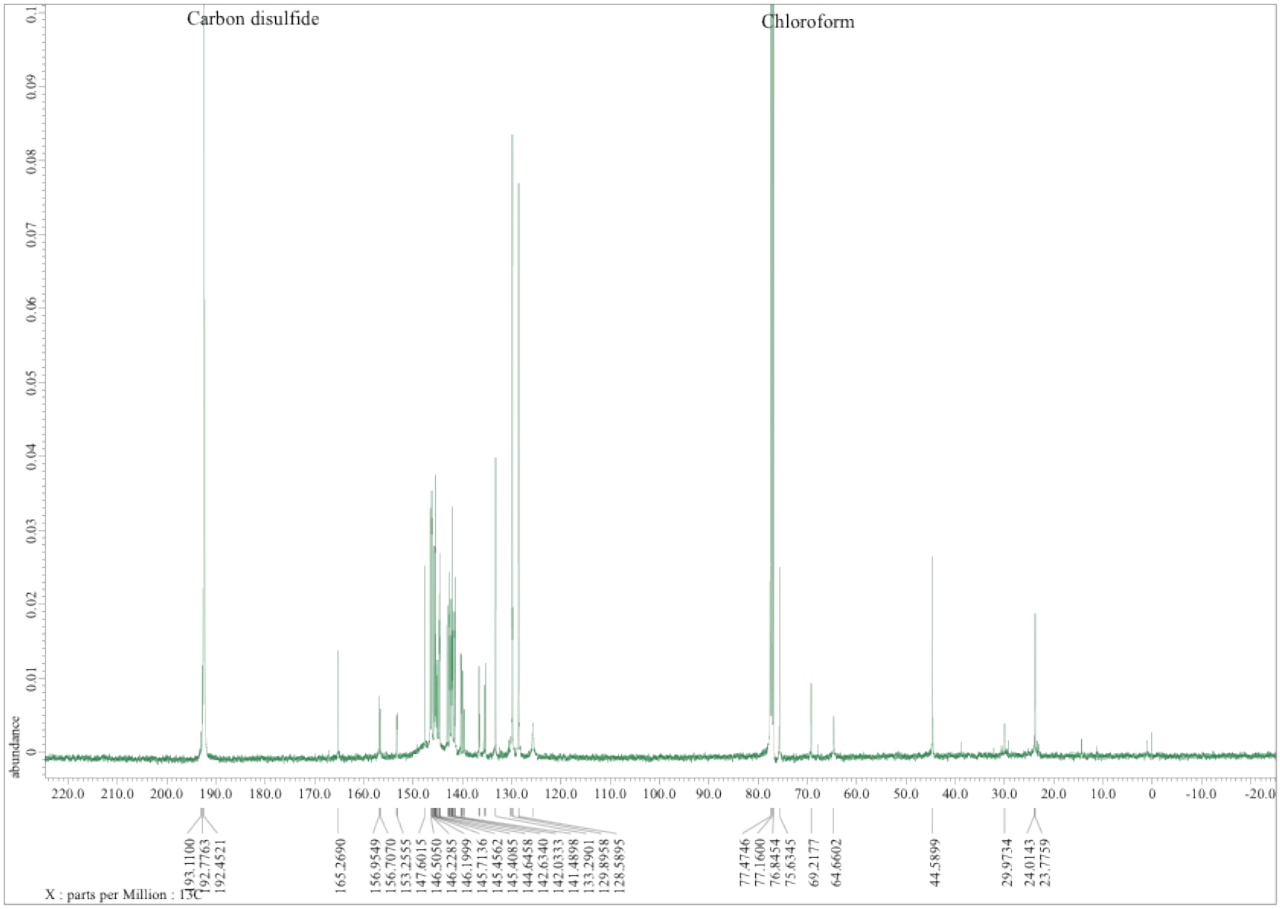

Fig. S22. ^{13}C NMR spectrum of **3b** recorded in $CDCl_3/CS_2$ (1:2).

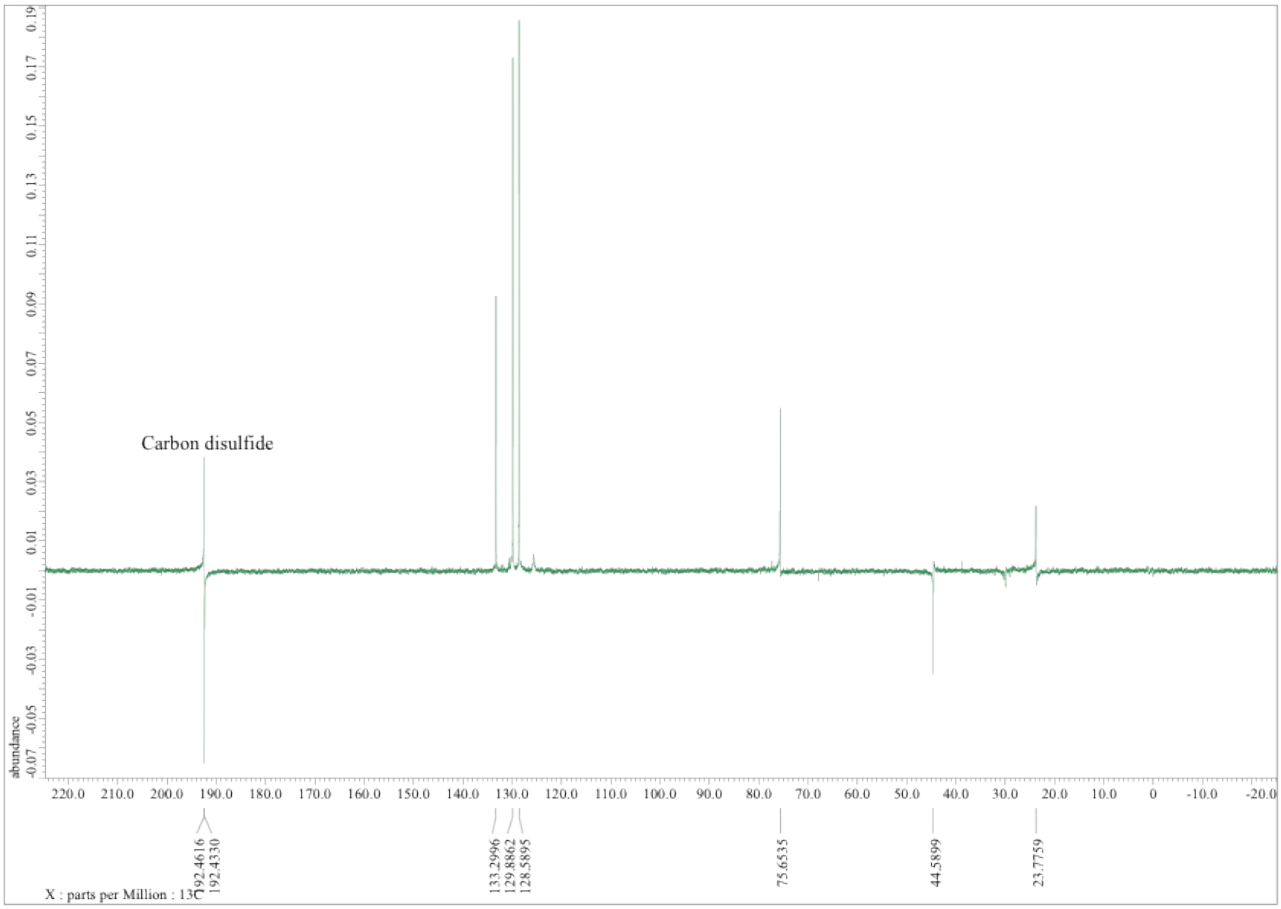

Fig. S23. Dept-135 NMR spectrum of **3b** recorded in $CDCl_3/CS_2$ (1:2).

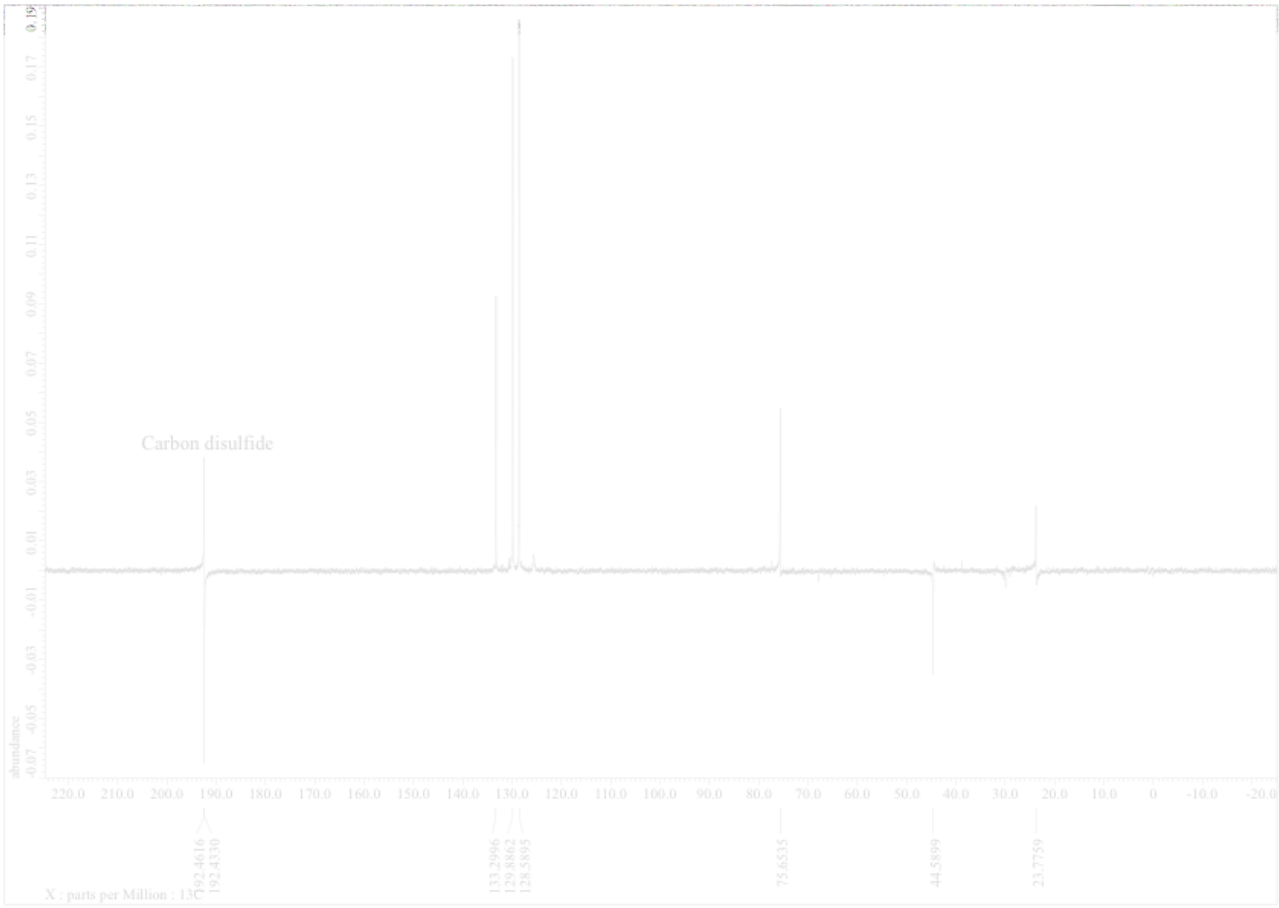

Fig. S24. Dept-135 NMR spectrum of **3b** recorded in $CDCl_3/CS_2$ (1:2).

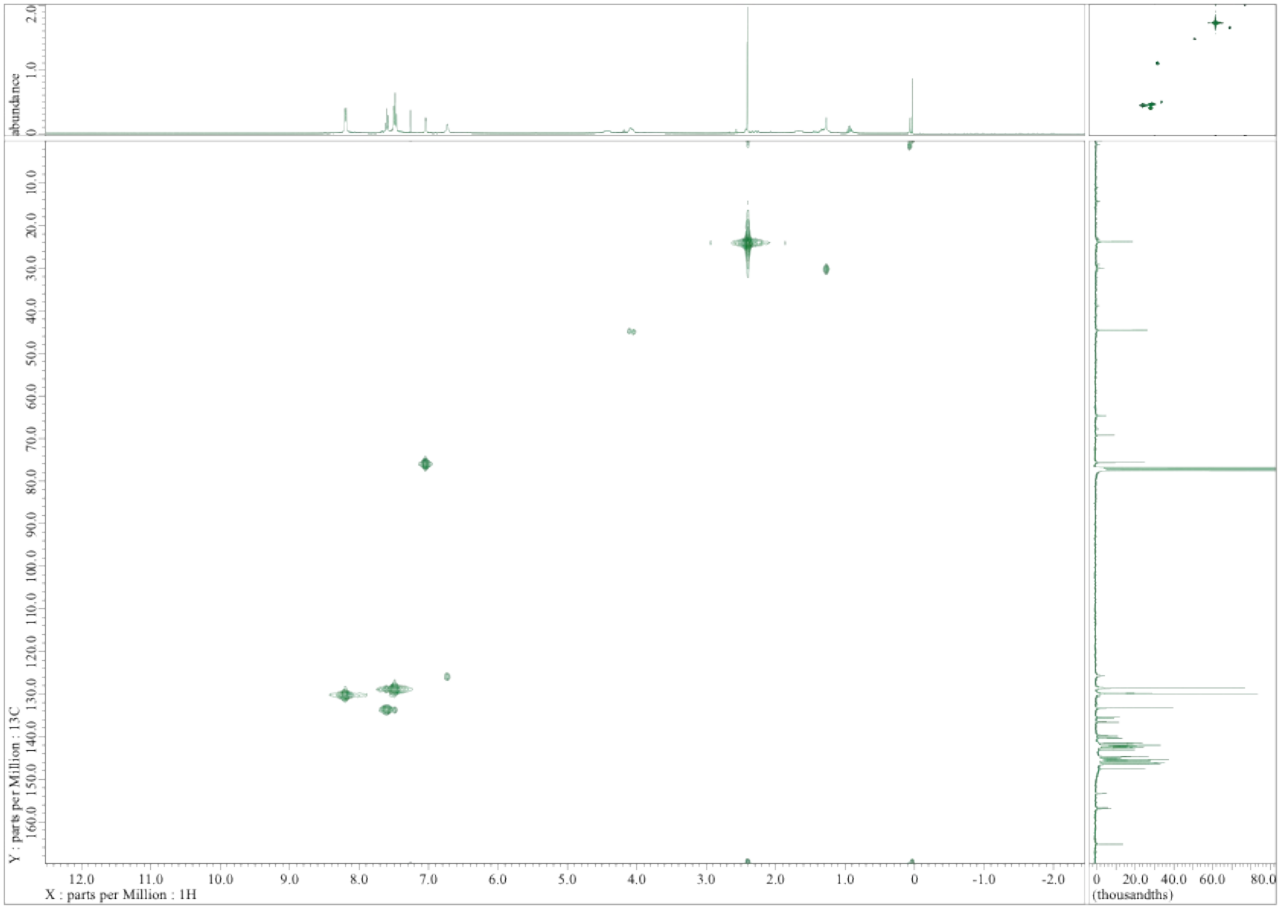

Fig. S25. HMQC NMR spectrum of **3b** recorded in $CDCl_3/CS_2$ (1:2).

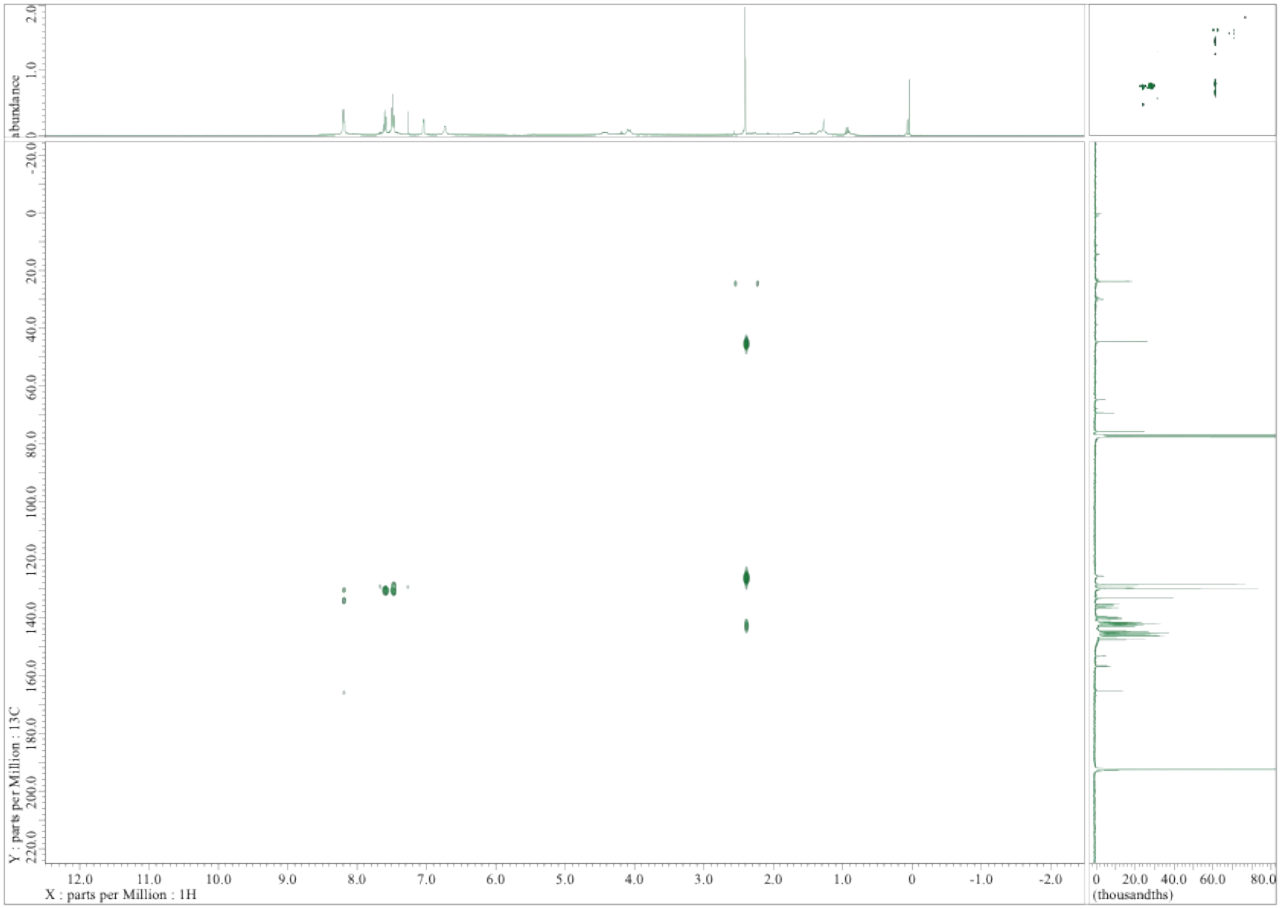

Fig. S26. HMBC NMR spectrum of **3b** recorded in $CDCl_3/CS_2$ (1:2).

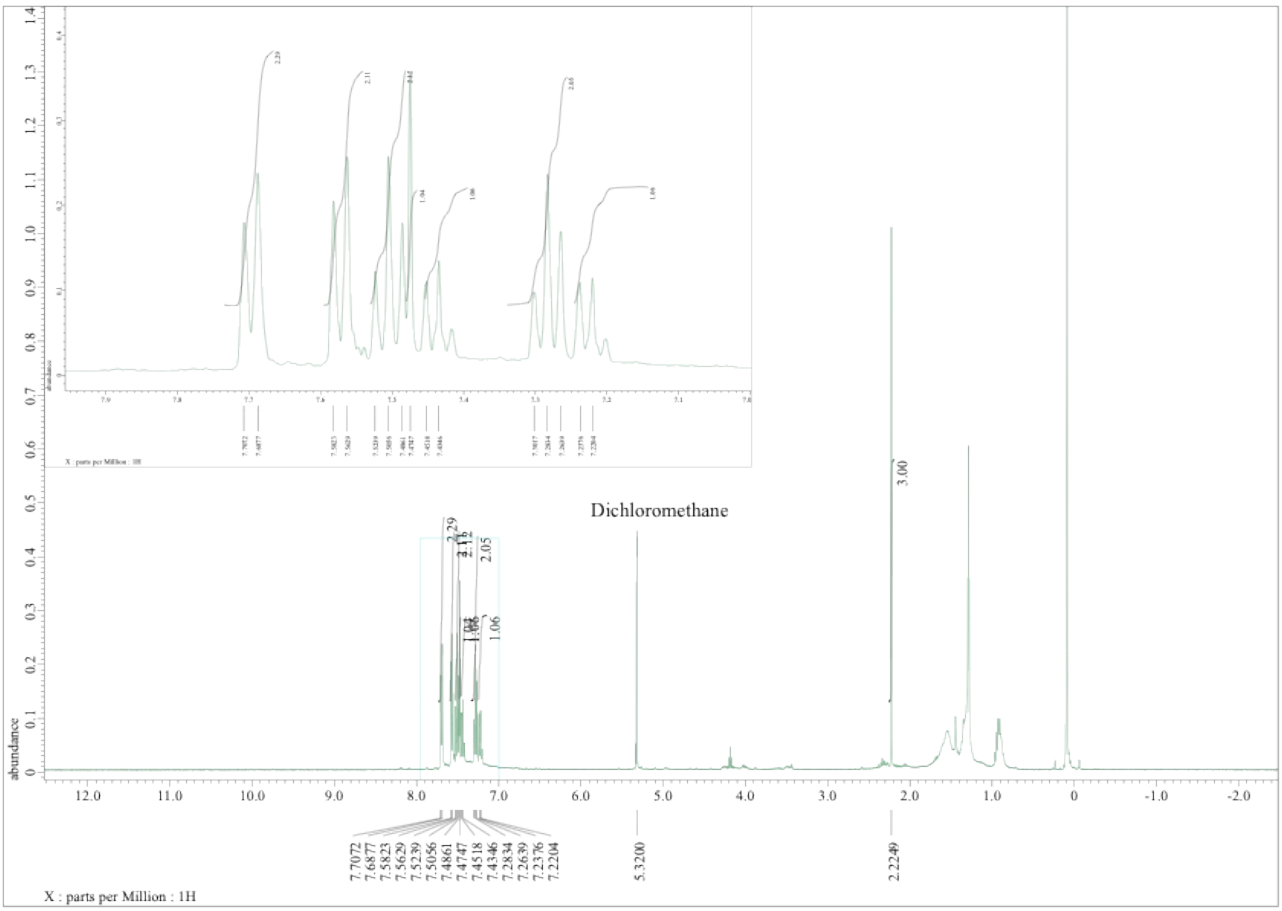

Fig. S27. ^{1}H NMR spectrum of **2c** recorded in CD_2Cl_2/CS_2 (3:1).

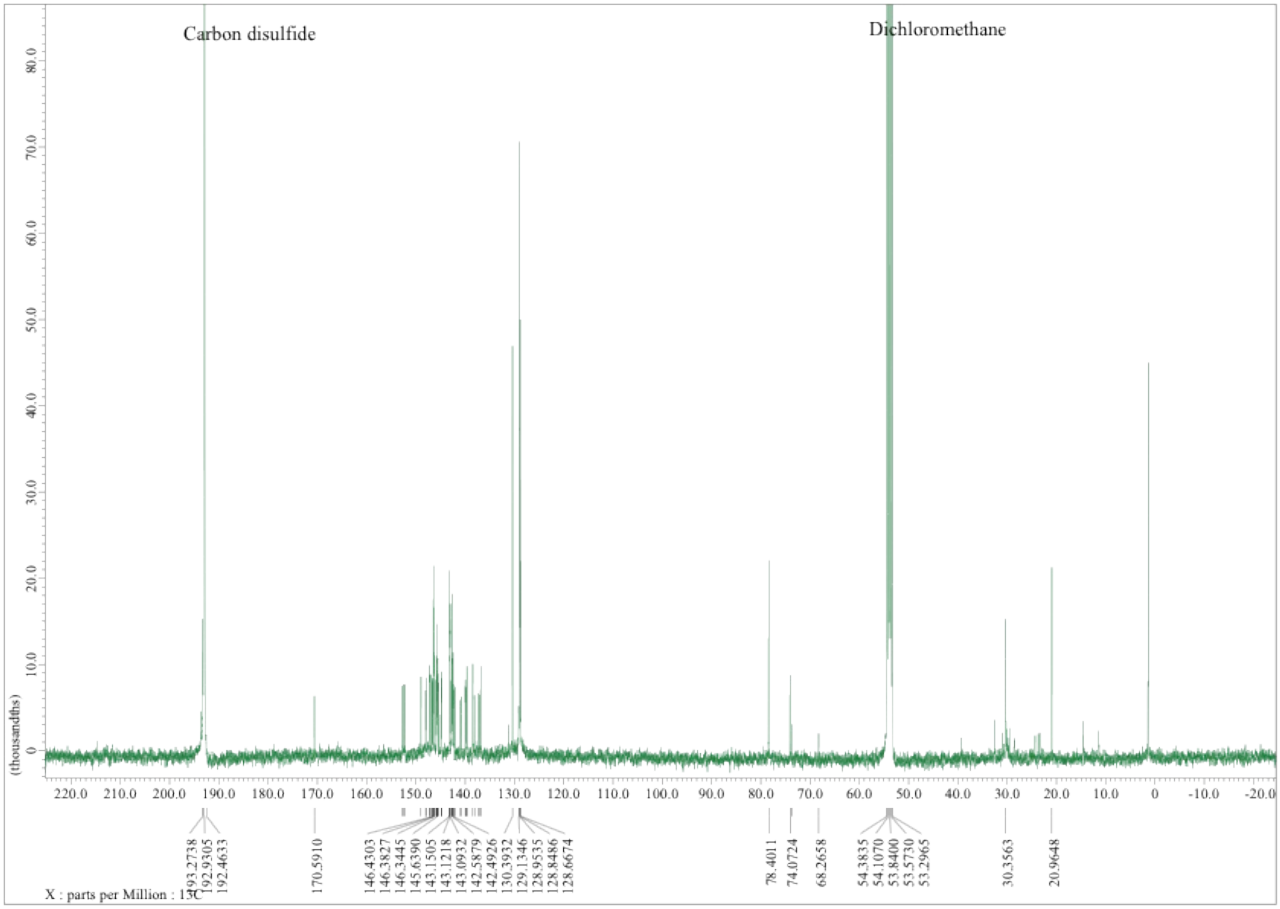

Fig. S28. ^{13}C NMR spectrum of **2c** recorded in CD_2Cl_2/CS_2 (3:1).

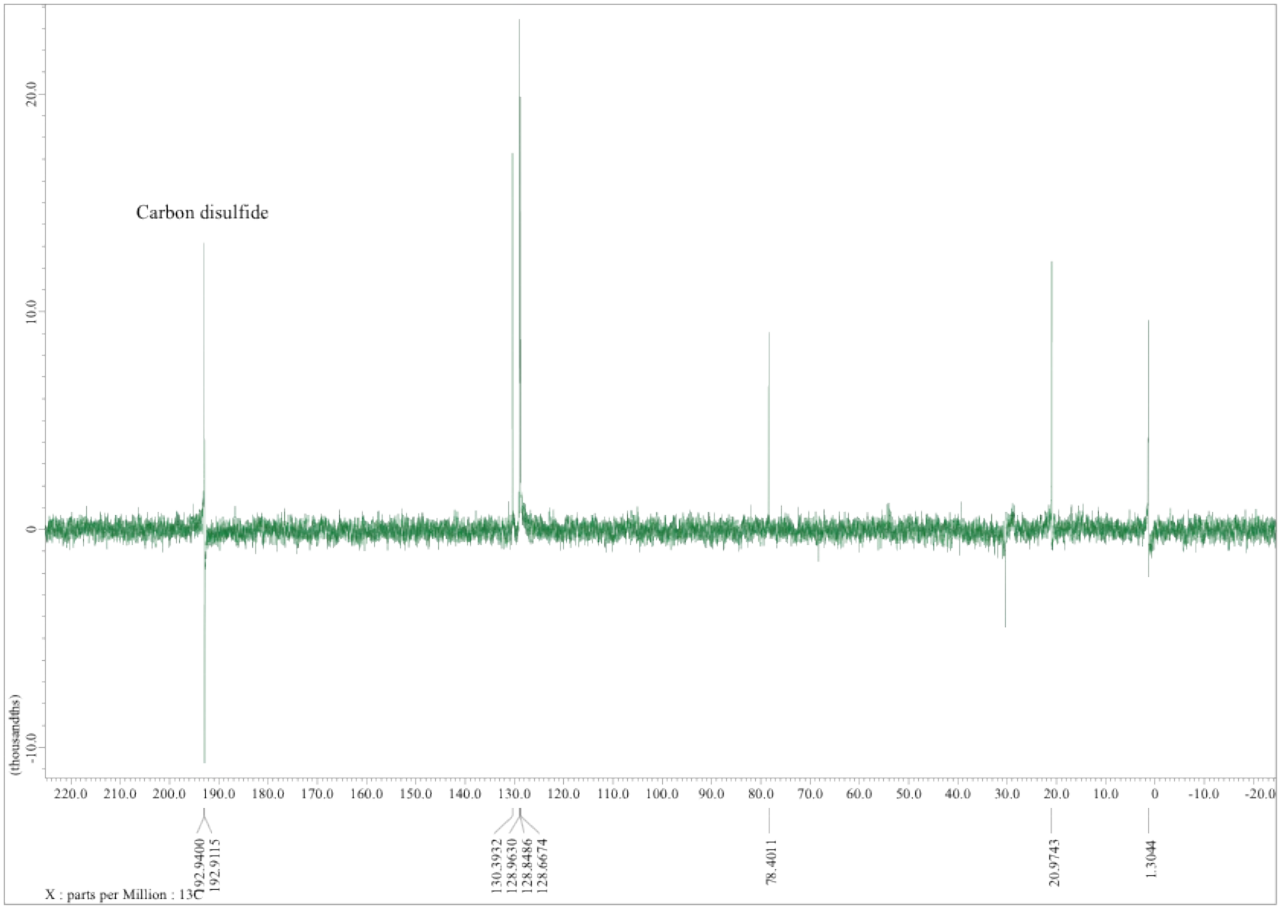

Fig. S29. Dept-135 NMR spectrum of **2c** recorded in CD_2Cl_2/CS_2 (3:1).

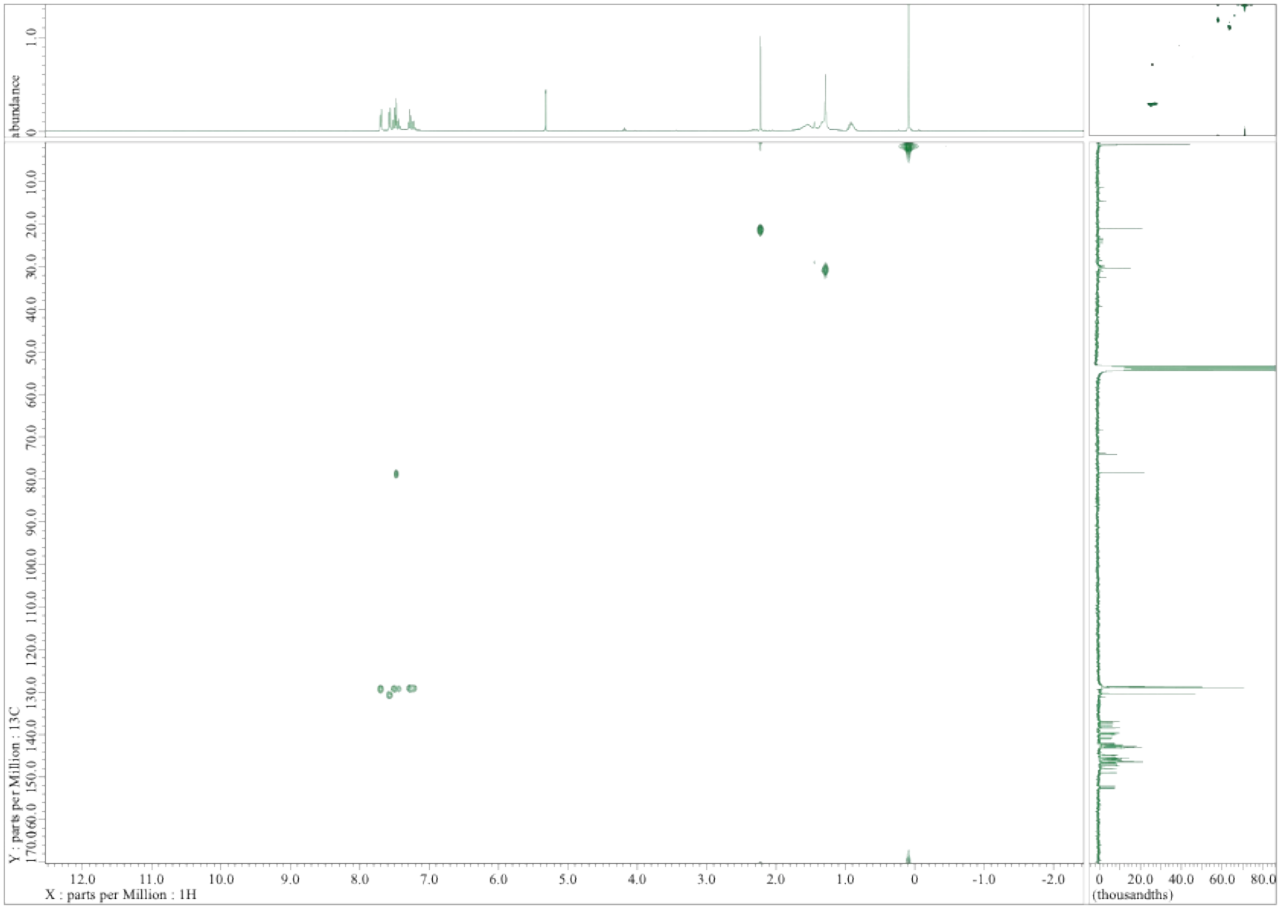

Fig. S30. HMQC NMR spectrum of **2c** recorded in CD_2Cl_2/CS_2 (3:1).

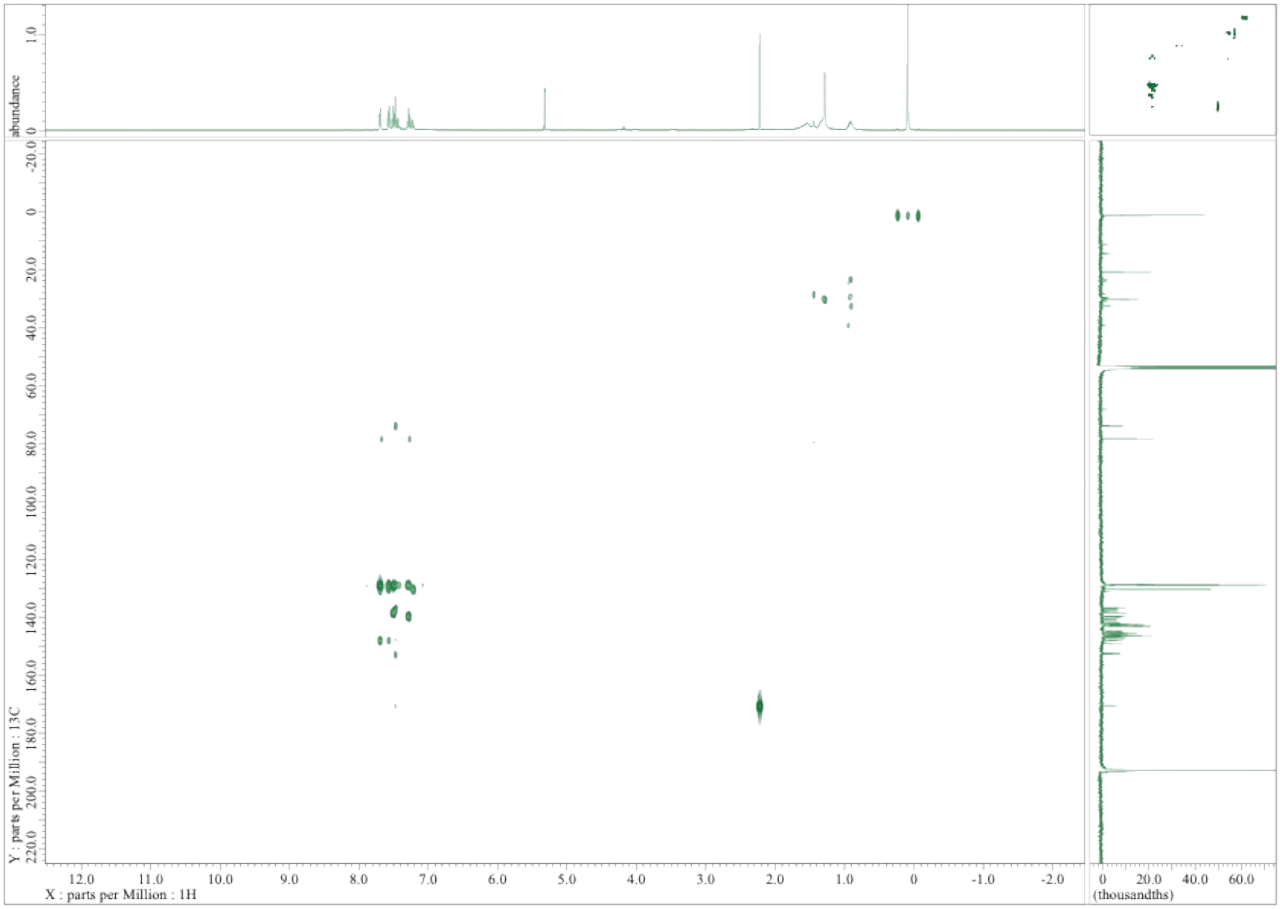

Fig. S31. HMBC NMR spectrum of **2c** recorded in CD_2Cl_2/CS_2 (3:1).

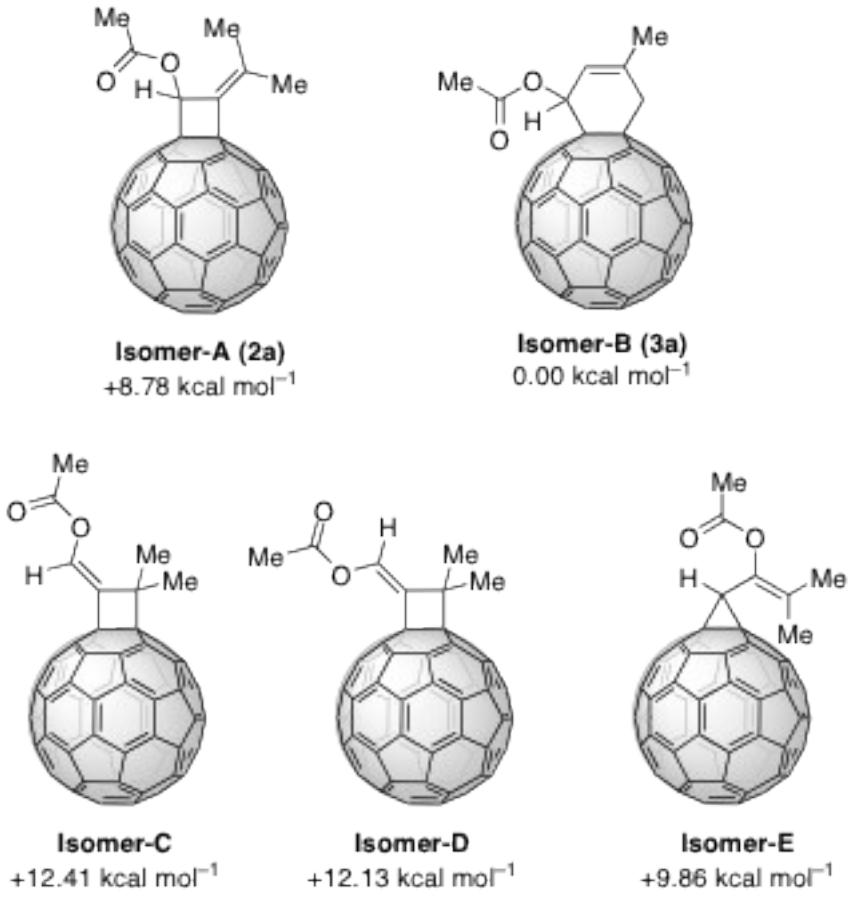

Fig. S32. Schematic structures and relative energies (in kcal mol^{-1}) of five possible structural isomers (Isomers A–E) of the cycloadduct where $R_1 = R_2 = Me$, calculated at the B3LYP/6-31G(d) level.

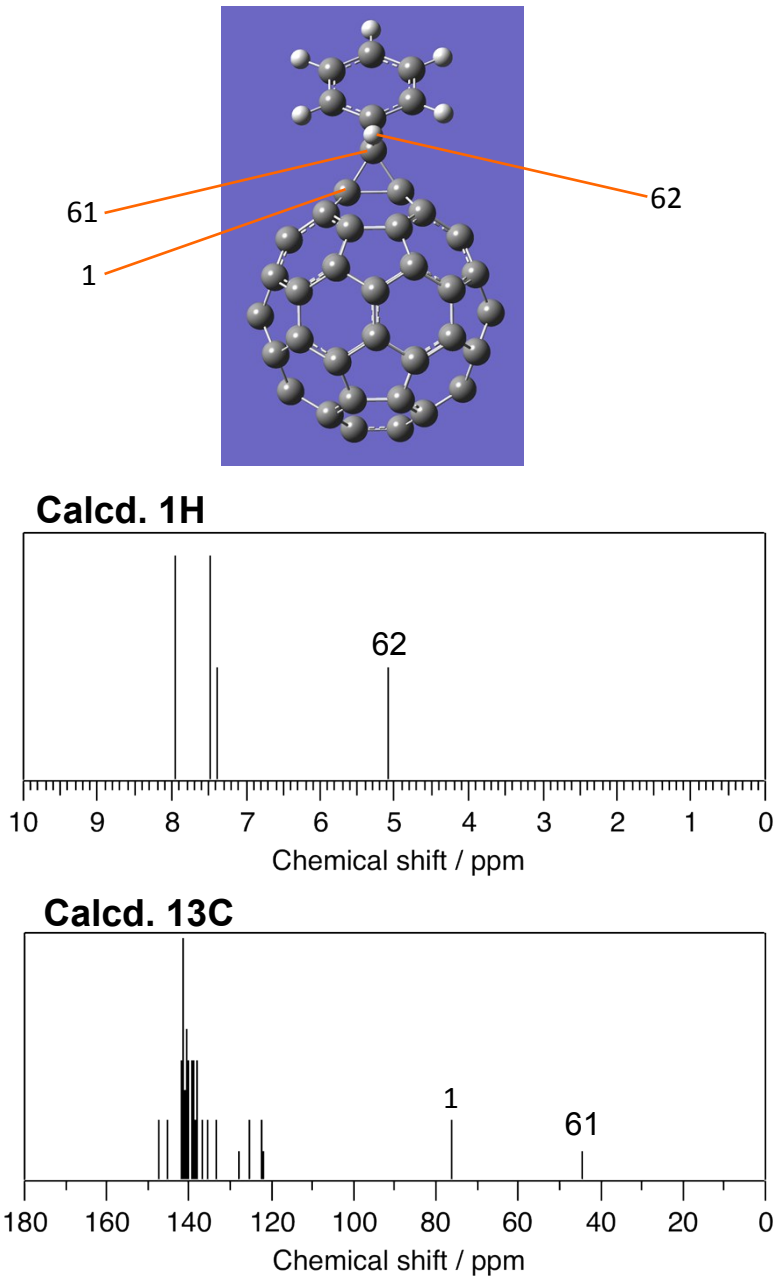

Fig. S33. Optimized structure of [6,6]-methanofullerene C_{60}(CHPh) and its NMR patterns as a model to assess validity of the basis sets and the functional of the presented calculations. The reported experimental NMR data for C_{60}(CHPh) are as follows; ^{1}H NMR (600 MHz, $CDCl_3$ /CS_2) δ = 5.38 (s, 1H), 7.44 (t, 1H), 7.50 (t, 2H), 7.93 (d, 2H) ppm (coupling constants are not presented in the reference9); ^{13}C NMR (150 MHz, $CDCl_3$ /CS_2) δ = 43.4, 75.0, 128.2, 128.6, 131.0, 132.7, 136.2, 138.2, 140.6, 140.9, 141.8, 141.9, 142.0, 142.4, 142.7, 142.8, 143.4, 143.5, 144.0, 144.1, 144.4, 144.5, 144.8, 144.9, 145.2, 145.3, 147.2, 149.3 ppm.9

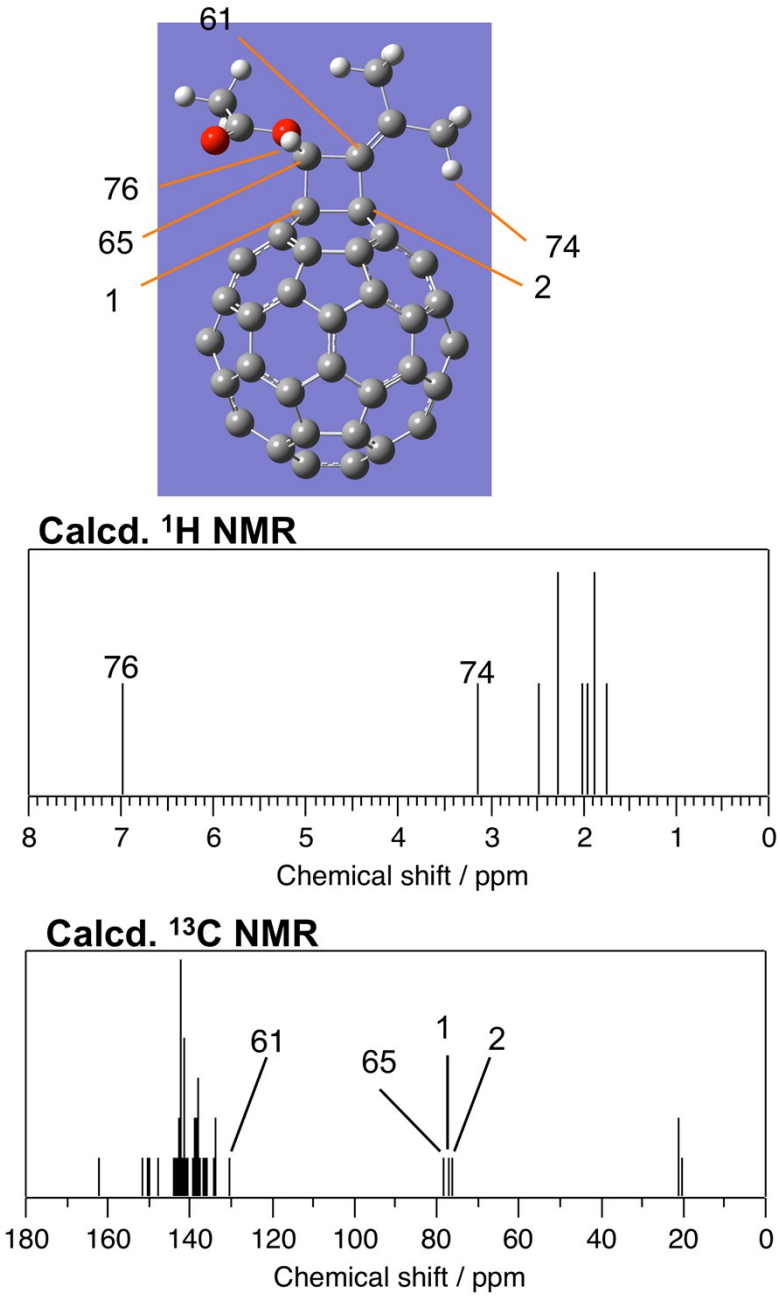

Fig. S34. Optimized structure of Isomer-A (that corresponds to **2a**) and its NMR patterns calculated at the B3LYP/6-31G(d) level.

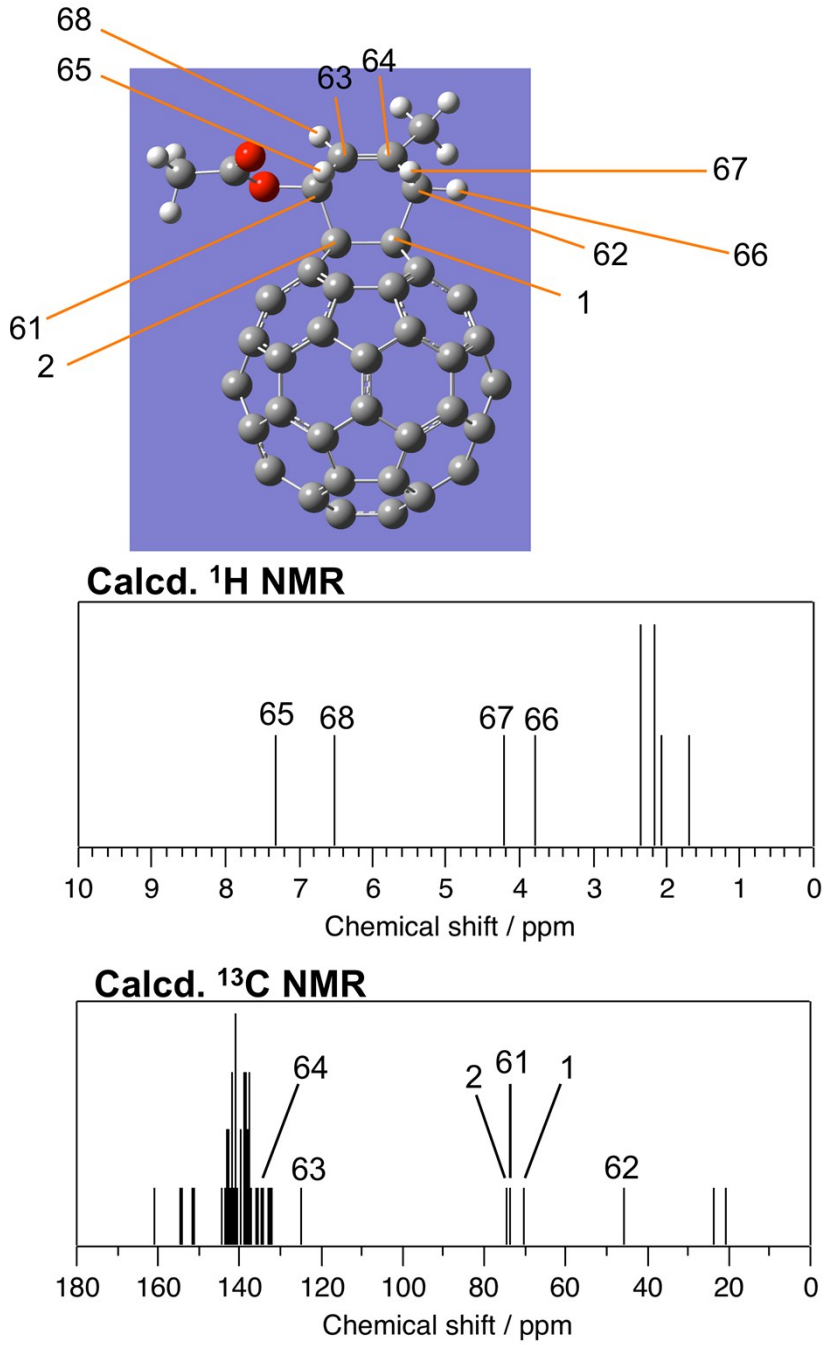

Fig. S35. Optimized structure of Isomer-B (that corresponds to **3a**) and its NMR patterns calculated at the B3LYP/6-31G(d) level.

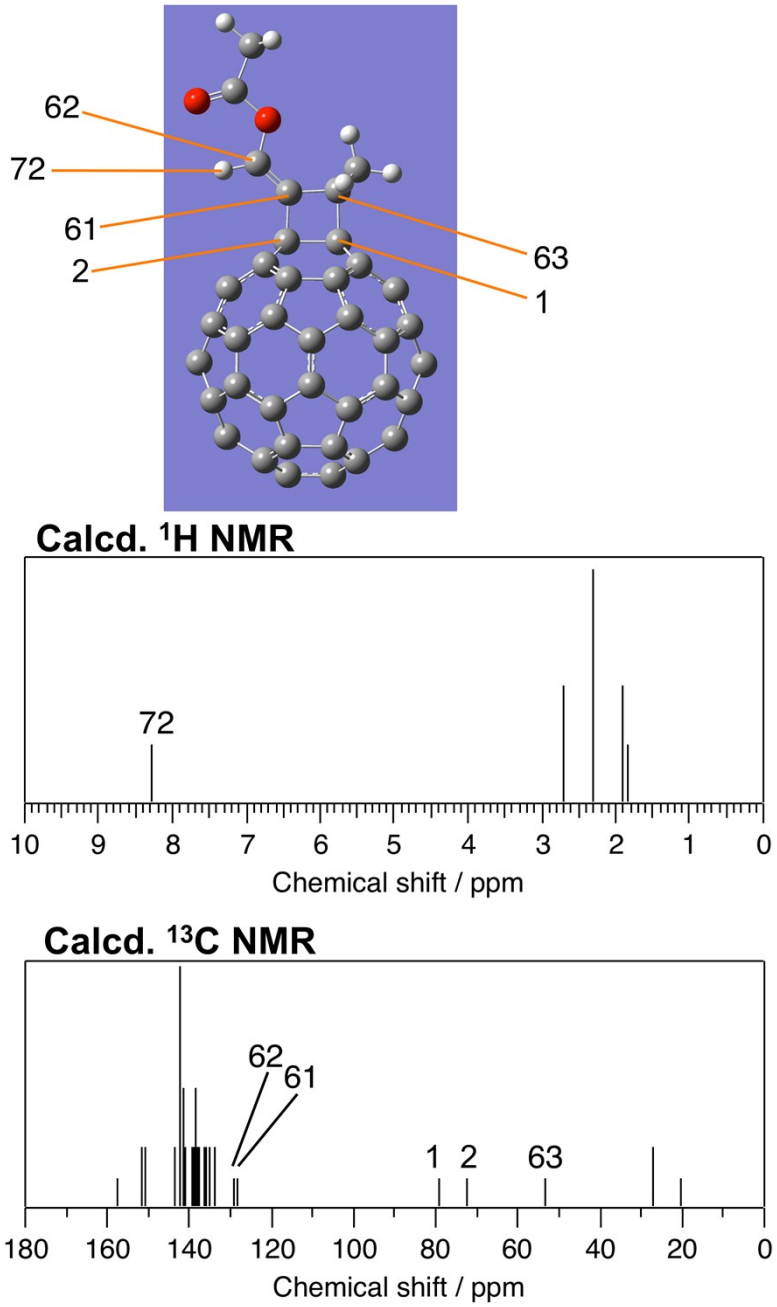

Fig. S36. Optimized structure of Isomer-C and its NMR patterns calculated at the B3LYP/6-31G(d) level.

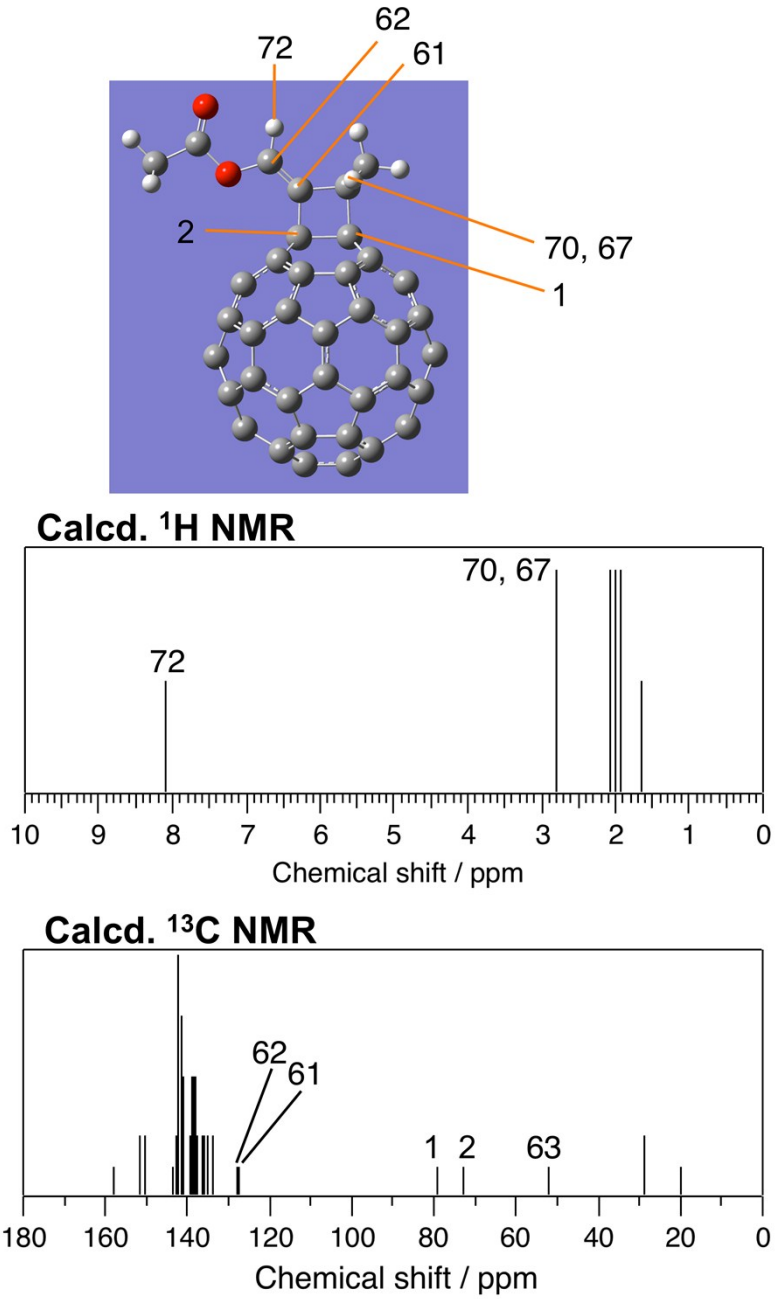

Fig. S37. Optimized structure of Isomer-D and its NMR patterns calculated at the B3LYP/6-31G(d) level.

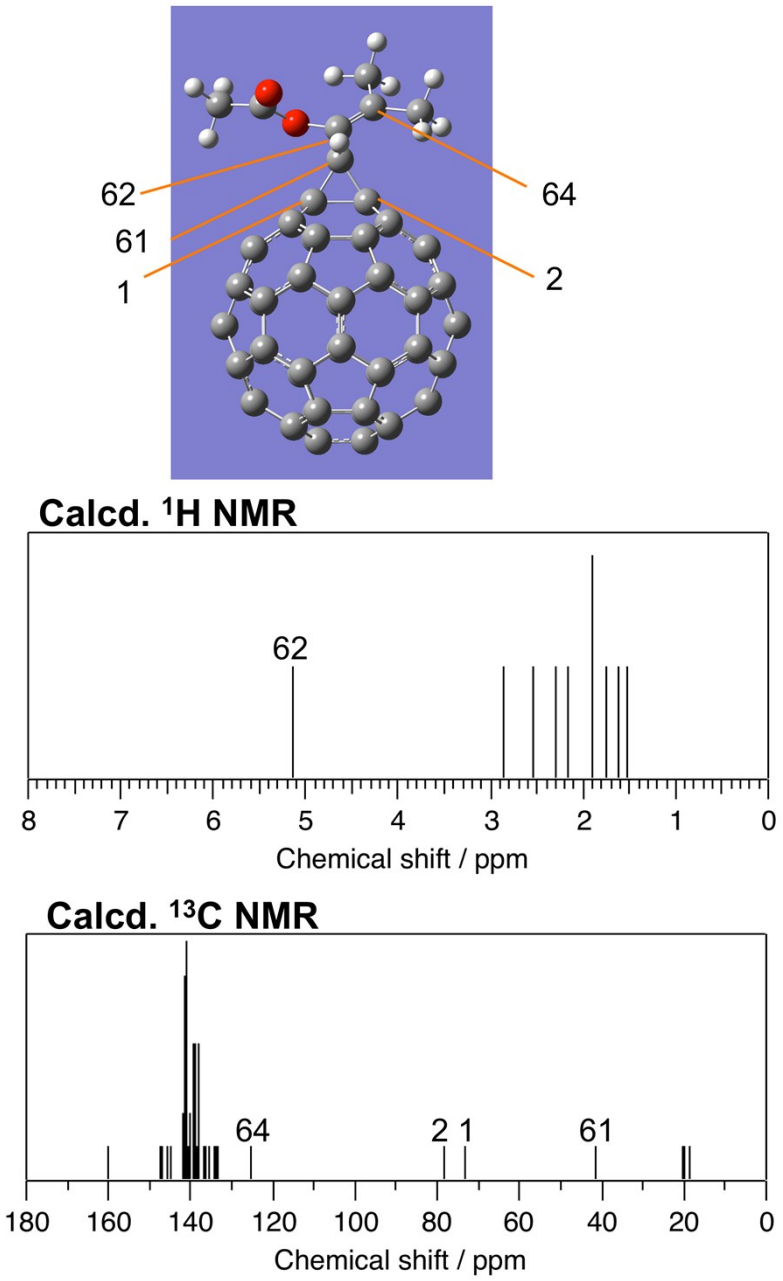

Fig. S38. Optimized structure of Isomer-E and its NMR patterns calculated at the B3LYP/6-31G(d) level.

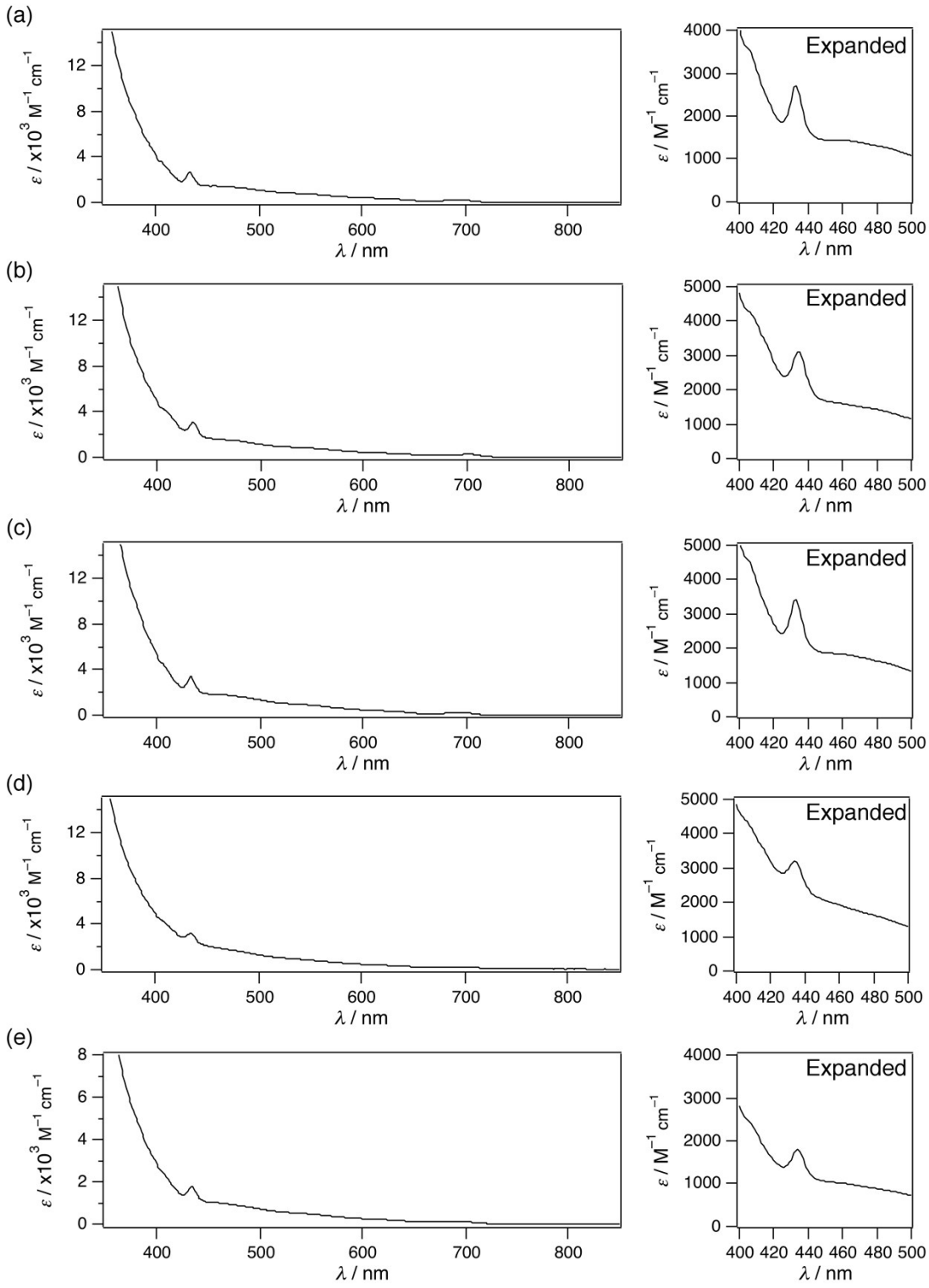

Fig. S39. Absorption spectra of (a) **2a**, (b) **3a**, (c) **2b**, (d) **3b**, and (e) **2c** in toluene.

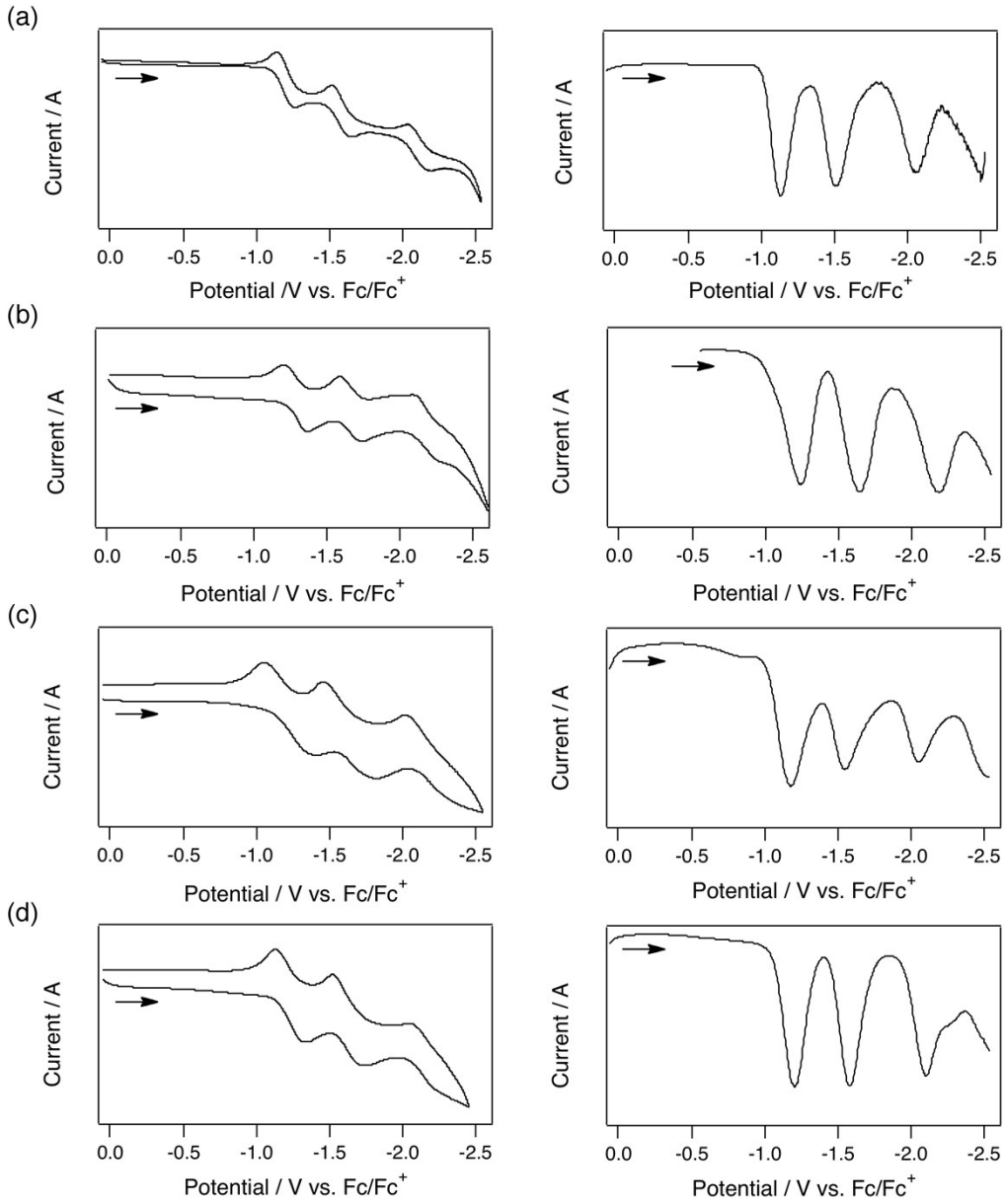

Fig. S40. CV (left) and DPV (right) curves of (a) **2a**, (b) **3a**, (c) **2b**, and (d) **3b**.

References (ESI)

1. L. Patiny and A. Borel, *J. Chem. Inf. Model.,* 2013, **53**, 1223–1228.
2. V. V. Pagar, A. M. Jadhav and R. S. Liu, *J. Am. Chem. Soc.,* 2011, **133**, 20728–20731.
3. A. Bartels, R. Mahrwald and K. Müller, *Adv. Synth. Catal.,* 2004, **346**, 483–485.
4. N. Marion, P. Carlqvist, R. Gealageas, P. de Frémont, F. Maseras and S. P. Nolan, *Chem. –Eur. J.,* 2007, **13**, 6437–6451.
5. R. C. Coocson, M. C. Cramp and P. J. Parsons, *J. Chem. Soc., Chem. Commun.,* 1980, 197–198.
6. M. J. Frisch, G. W. Trucks, H. B. Schlegel, G. E. Scuseria, M. A. Robb, J. R. Cheeseman, G. Scalmani, V. Barone, B. Mennucci, G. A. Petersson, H. Nakatsuji, M. Caricato, X. Li, H. P. Hratchian, A. F. Izmaylov, J. Bloino, G. Zheng, J. L. Sonnenberg, M. Hada, M. Ehara, K. Toyota, R. Fukuda, J. Hasegawa, M. Ishida, T. Nakajima, Y. Honda, O. Kitao, H. Nakai, T. Vreven, J. A. Montgomery Jr., J. E. Peralta, F. Ogliaro, M. Bearpark, J. J. Heyd, E. Brothers, K. N. Kudin, V. N. Staroverov, R. Kobayashi, J. Normand, K. Raghavachari, A. J. Rendell, C. Burant, S. S. Iyengar, J. Tomasi, M. Cossi, N. Rega, J. M. Millam, M. Klene, J. E. Knox, J. B. Cross, V. Bakken, C. Adamo, J. Jaramillo, R. Gomperts, R. E. Stratmann, O. Yazyev, A. J. Austin, R. Cammi, C. Pomelli, J. W. Ochterski, R. L. Martin, K. Morokuma, V. G. Zakrzewski, G. A. Voth, P. Salvador, J. J. Dannenberg, S. Dapprich, A. D. Daniels, O. Farkas, J. B. Foresman, J. V. Ortiz, J. Cioslowski and D. J. Fox, *Gaussian 09*, revision D.01; Gaussian, Inc.: Wallingford, CT, 2009.
7. W. J. Hehre, R. Ditchfield and J. A. Pople,*J. Chem. Phys.,* 1972, **56**, 2257−2261.
8. *CONFLEX 7*, H. Goto, S. Obata, N. Nakayama and K. Ohta, CONFLEX Corporation, Tokyo, Japan, 2012.
9. M. Zheng, F. Li, Z. Shi, X. Gao and K. M. Kadish, *J. Org. Chem.,* 2007, **72**, 2538–2542.